Cell Reports

Article

MicroRNA-29 specifies age-related differences in the CD8+ T cell immune response

Graphical abstract

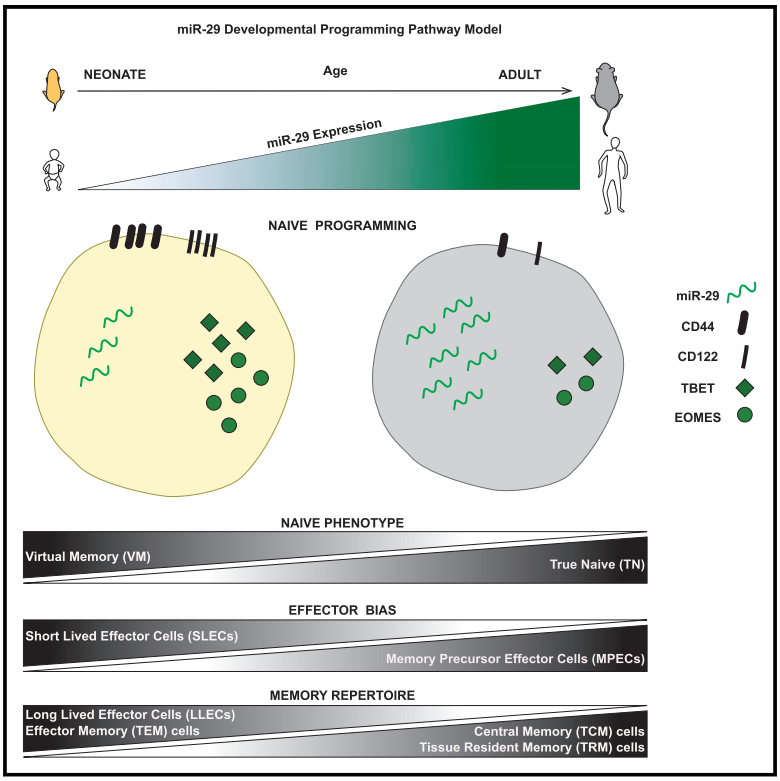

Highlights

- miR-29 is required for the normal memory response of adult CD8+ T cells
- miR-29 acts in naive cells to pre-program the immune response
- Loss of miR-29 in adult cells impairs memory functions, mimicking neonatal cells
- Gain of miR-29 in neonatal cells improves memory response

Authors

Kristel J. Yee Mon, Hongya Zhu, Ciarán W.P. Daly, ..., Minh T.N. Le, Brian D. Rudd, Andrew Grimson

Correspondence

agrimson@cornell.edu (A.G.), bdr54@cornell.edu (B.D.R.)

In brief

Yee Mon et al. show that a small noncoding RNA, microRNA-29, specifies how CD8+ T cells, in humans and mice, will respond to infection even prior to encountering antigen. This pre-programing underlies the fundamental differences between adult and neonatal CD8+ T cells, which express miR-29 at different levels.

Yee Mon et al., 2021, Cell Reports *37*, 109969
November 9, 2021
https://doi.org/10.1016/j.celrep.2021.109969

CellPress

Cell Reports

CellPress
OPEN ACCESS

Article

MicroRNA-29 specifies age-related differences in the CD8+ T cell immune response

Kristel J. Yee Mon,[1] Hongya Zhu,[2] Ciarán W.P. Daly,[2] Luyen T. Vu,[2,3] Norah L. Smith,[1] Ravi Patel,[2] David J. Topham,[4] Kristin Scheible,[5] Kondwani Jambo,[6,7] Minh T.N. Le,[3] Brian D. Rudd,[1,*] and Andrew Grimson[2,8,*]

[1]Department of Microbiology and Immunology, Cornell University, Ithaca, NY 14853, USA
[2]Department of Molecular Biology and Genetics, Cornell University, Ithaca, NY 14853, USA
[3]Department of Pharmacology and Institute for Digital Medicine, Yong Loo Lin School of Medicine, National University of Singapore, Singapore
[4]Department of Microbiology and Immunology, University of Rochester, Rochester, NY 14642, USA
[5]Department of Pediatrics, Division of Neonatology, University of Rochester, Rochester, NY 14642, USA
[6]Department of Clinical Sciences, Liverpool School of Tropical Medicine, Liverpool, UK
[7]Malawi-Liverpool-Wellcome Trust Clinical Research Programme, University of Malawi College of Medicine, Blantyre, Malawi
[8]Lead contact
*Correspondence: agrimson@cornell.edu (A.G.), bdr54@cornell.edu (B.D.R.)
https://doi.org/10.1016/j.celrep.2021.109969

SUMMARY

MicroRNAs (miRNAs) have emerged as critical regulators of cell fate in the CD8+ T cell response to infection. Although there are several examples of miRNAs acting on effector CD8+ T cells after infection, it is unclear whether differential expression of one or more miRNAs in the naive state is consequential in altering their long-term trajectory. To answer this question, we examine the role of miR-29 in neonatal and adult CD8+ T cells, which express different amounts of miR-29 only prior to infection and adopt profoundly different fates after immune challenge. We find that manipulation of miR-29 expression in the naive state is sufficient for age-adjusting the phenotype and function of CD8+ T cells, including their regulatory landscapes and long-term differentiation trajectories after infection. Thus, miR-29 acts as a developmental switch by controlling the balance between a rapid effector response in neonates and the generation of long-lived memory in adults.

INTRODUCTION

MicroRNAs (miRNAs) are small noncoding RNAs which regulate much of the transcriptome in mammals. Mammalian genomes contain hundreds of conserved miRNAs; cumulatively, the scope of miRNA-mediated regulation indicates that most gene regulatory pathways incorporate miRNAs (Bartel, 2009). Canonically, miRNAs recognize their target mRNAs by base pairing between the 5′ region of the miRNA, a 6–8 nucleotide sequence called the seed, and a cognate target site in the 3′ untranslated region. Effective targeting results predominantly in mRNA destabilization (Bartel, 2018). Because targeting is specified by the seed, miRNAs sharing the same seed are grouped into families, with individual members often serving redundant functions due to their common target repertoire (Bartel, 2009).

In the immune system, miRNAs contribute to a multitude of cellular functions (O'Connell et al., 2010). In T cells, miRNAs play an integral role in thymic maturation (Podshivalova and Salomon, 2013), homeostasis, survival, activation (Bronevetsky et al., 2013; Zhang and Bevan, 2010; Dooley et al., 2013), effector and memory cell differentiation (Kroesen et al., 2015; Liang et al., 2015; Smith et al., 2015), and establishment of activation thresholds (Liston et al., 2012). One miRNA, miR-29, has been studied in CD4+ T cells (Wells, Pobezinskaya and Pobezinsky, 2020) but minimally in CD8+ T cells. In CD4+ T cells, miR-29 regulates Notch (Chandiran et al., 2018), T-box transcription factors, and inflammatory cytokine production (Steiner et al., 2011, Ma et al., 2011) and also controls polarization after infection (Chandiran et al., 2018).

The major functions of CD8+ T cells are to secrete effector molecules that kill intracellular pathogens, and cytokines that mobilize immune cells to respond to pathogens (Butz and Bevan, 1998; Whitmire et al., 2005). Neonatal CD8+ T cells exhibit profound functional differences to their adult counterparts (Rudd, 2020), a phenomenon that extends to other immune cells (Yu et al., 2018; Basha, Surendran and Pichichero, 2014; Philbin and Levy, 2009). Neonatal CD8+ T cells are derived from fetal liver rather than bone marrow stem cells, have different metabolic programs, increased secretion of cytolytic molecules, and have a higher proliferative and activation capacity (Smith et al., 2018; Wang et al., 2016; Tabilas et al., 2019; Reynaldi et al., 2016). Moreover, neonatal CD8+ T cells have a propensity to become terminally differentiated at the cost of forming immunological memory (Smith et al., 2014). Thus, identifying the regulatory programs that differentiate adult and neonatal CD8+ T cells remains a key question for understanding the immune system.

Multiple miRNAs exhibit dynamic expression during thymic development of CD8+ T cells, and play a role in balancing memory and effector CD8+ T cell formation after infection in adults

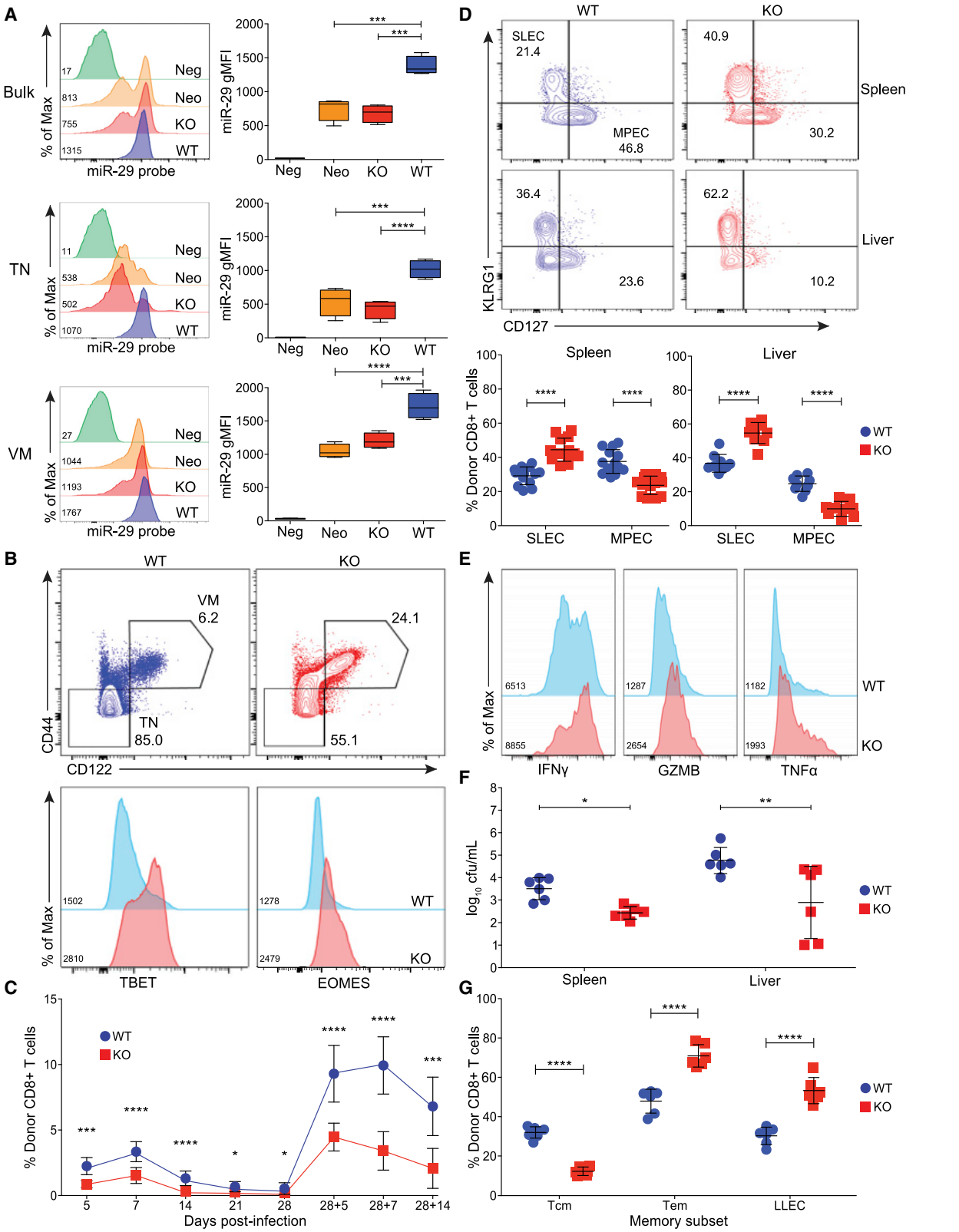

(legend on next page)

(Zhang et al., 2018; Muljo et al., 2005; Wu et al., 2007; Wu et al., 2012). In adult mouse naive CD8+ T cells, miR-29a is among the most highly expressed miRNAs, and is the most highly expressed member of the miR-29 family (miR-29a, b-1, b-2 and c) (Wissink et al., 2015). Moreover, miR-29 is developmentally regulated; miR-29 expression is high in adult naive CD8+ T cells, in both mice and humans, but lower in neonatal cells (Wissink et al., 2015). Importantly, adult and neonatal naive CD8+ T cell transcriptomes exhibit reciprocal changes in expression of likely targets of miR-29 (Wissink et al., 2015), implying that miR-29 specifies regulatory differences in an age-related fashion, with a set of targets expressed at higher levels in neonatal CD8+ T cells concomitant with low miR-29 levels (Wissink et al., 2015). Possible miR-29 targets include *Tbet, Eomes, Dnmt3a* and *IFNγ,* regulators that define CD8+ T cell fate (Wissink et al., 2015; Ma et al., 2011; Steiner et al., 2011). Thus, we hypothesized that miR-29 acts as a developmental switch prior to infection that specifies alternative gene regulatory programs in naive cells, which delineate adult and neonatal CD8+ T cell fates by controlling the balance between the effector response, characteristic of neonatal cells, and the generation of memory cells, observed in adults (Wissink et al., 2015).

A number of studies have linked the fate of CD8+ T cells to specific miRNAs that arise after infection. For example, miR-17-92 is upregulated in effector cells and drives proliferation by enhancing PI3K-Akt-mTOR signaling (Wu et al., 2012), while miR-155 expression supports CD8+ T cell expansion by blunting the antiproliferative effect of type I interferons after infection (Gracias et al., 2013). Furthermore, miR-146a is upregulated in effector cells and facilitates resolution of the CD8+ T cell response to infection (Yang et al., 2012). Collectively, these reports have led to a prevailing notion that the CD8+ T cell trajectory during infection is governed by the expression of miRNAs that are abundant in effector cells. Thus, an important unanswered question is whether differential miRNA expression in naive CD8+ T cells is consequential to downstream function.

Here, we examined the significance and role of miR-29 in primary human and mouse naive CD8+ T cells. Our results demonstrate that miR-29 expression in adult naive cells specifies a gene regulatory program that promotes immune memory. In contrast, low miR-29 expression in neonatal CD8+ T cells impairs a robust memory response. Taken together, this study shows that miR-29 regulates the CD8+ T cell response to infection by establishing a gene regulatory program prior to infection, which governs the developmental trajectory of T cells after infection. Our findings also raise the possibility that miRNAs can be used as biomarkers for predicting vaccine efficacy and infection outcomes at different stages of life.

RESULTS

miR-29 is required for normal CD8+ T cell function in adult mice

In mice and humans, adult naive CD8+ T cells express high levels of miR-29, while naive neonatal cells express lower levels (Wissink et al., 2015). Here, we examined the functional relevance of adult miR-29 expression using Cre-mediated conditional deletion of a floxed miR-29ab1 locus in gBT-I mice, which express a TCR specific for the HSV-1 glycoprotein $B_{498-505}$ epitope (Mueller et al., 2002). We used PrimeFlow to examine miR-29 in naive neonatal CD8+ T cells, and in adult cells with floxed miR-29ab1, comparing littermates with and without Cre. As expected, miR-29 levels are highest in adult cells with wild-type miR-29 (WT) and lowered upon miR-29ab1 excision (KO), mimicking neonatal levels (Figure 1A). These differences in miR-29 levels also exist in true naive (TN) and virtual memory (VM) subsets (Figure 1A). However, the presence of miR-29 in Cre+ adults, albeit at lowered levels, implies incomplete excision of miR-29ab1, which we confirmed using a PCR assay that indicated ~45%–75% excision (Figure S1A). We conclude that our mouse model reduces miR-29 levels, approximating neonatal levels in adult CD8+ T cells.

A characteristic difference between neonatal and adult CD8+ T cells is found within the naive pool; neonates contain a higher proportion of VM cells and a smaller proportion of TN cells (Wang et al., 2016). We examined the impact of reduced miR-29 levels in adults and as expected, the pool was comprised predominantly of TN cells in control littermates (Cre-), whereas reduced miR-29 depleted the TN proportion and elevated the VM population (Figures 1B and S1B), a phenotype characteristic of neonates (Wang et al., 2016; Smith et al., 2018). Reducing miR-29 increased expression of the transcription factors Tbet and Eomes, which are expressed at higher levels in neonates (Smith et al., 2014) and are predicted miR-29 targets (Wissink et al.,

Figure 1. miR-29 is required for normal CD8+ T cell function

(A) PrimeFlow assay of miR-29a (y axis - geometric mean fluorescence intensity, gMFI) and histograms of miR-29a modal fluorescence intensities from bulk (top) and true naive and virtual memory subsets (middle and bottom, respectively) splenic naive CD8+ T cells and negative control (Neg; miR-29 probe omitted), plotting ± SD of 2 experiments with 3 mice per group per experiment, ***$p \leq 0.001$; unpaired Student's t test.

(B) (Top) Contour plots of TN and VM splenic CD8+ T cells from WT and KO mice. (Bottom) Histograms of Tbet and Eomes expression.

(C) Kinetics of WT and KO CD8+ T cells throughout VACV-gB primary infection (5-28 dpi) and LM-gB secondary infection. Data represent mean ± SD of 2 experiments with 8-10 mice per group per experiment; 2-WAY ANOVA, *$p \leq 0.05$, ***$p \leq 0.001$, ****$p \leq 0.0001$.

(D) Representative contour plots (top) of WT and KO SLEC and MPEC CD8+ T cells at 7 dpi, with quantification (bottom), plotting mean ± SD of 2 experiments with 6-7 mice per group per experiment; 2-WAY ANOVA, ****$p \leq 0.0001$.

(E) Histograms of IFNγ, GZMB and TNFα after peptide restimulation of CD8+ T cells at 7 dpi.

(F) Pathogen burden quantification of *Listeria*-gB colony forming units (y axis) at 3 dpi in spleen and liver homogenate, plotting mean ± SD of 2 experiments with 3 mice per group per experiment; 2-WAY ANOVA, *$p \leq 0.05$, **$p \leq 0.01$.

(G) Quantification of CD8+ T cell memory subsets Tcm (CD62L+ CD127+), Tem (CD62L- CD127+) and LLEC (KLRG1+ CD62L- CD43- CD27-) at 35 dpi, plotting mean ± SD of 2 experiments with 3 mice per group per experiment; 2-WAY ANOVA, ****$p \leq 0.0001$.

Representative gMFI values of respective groups indicated as a histogram inset.

See also Figure S1.

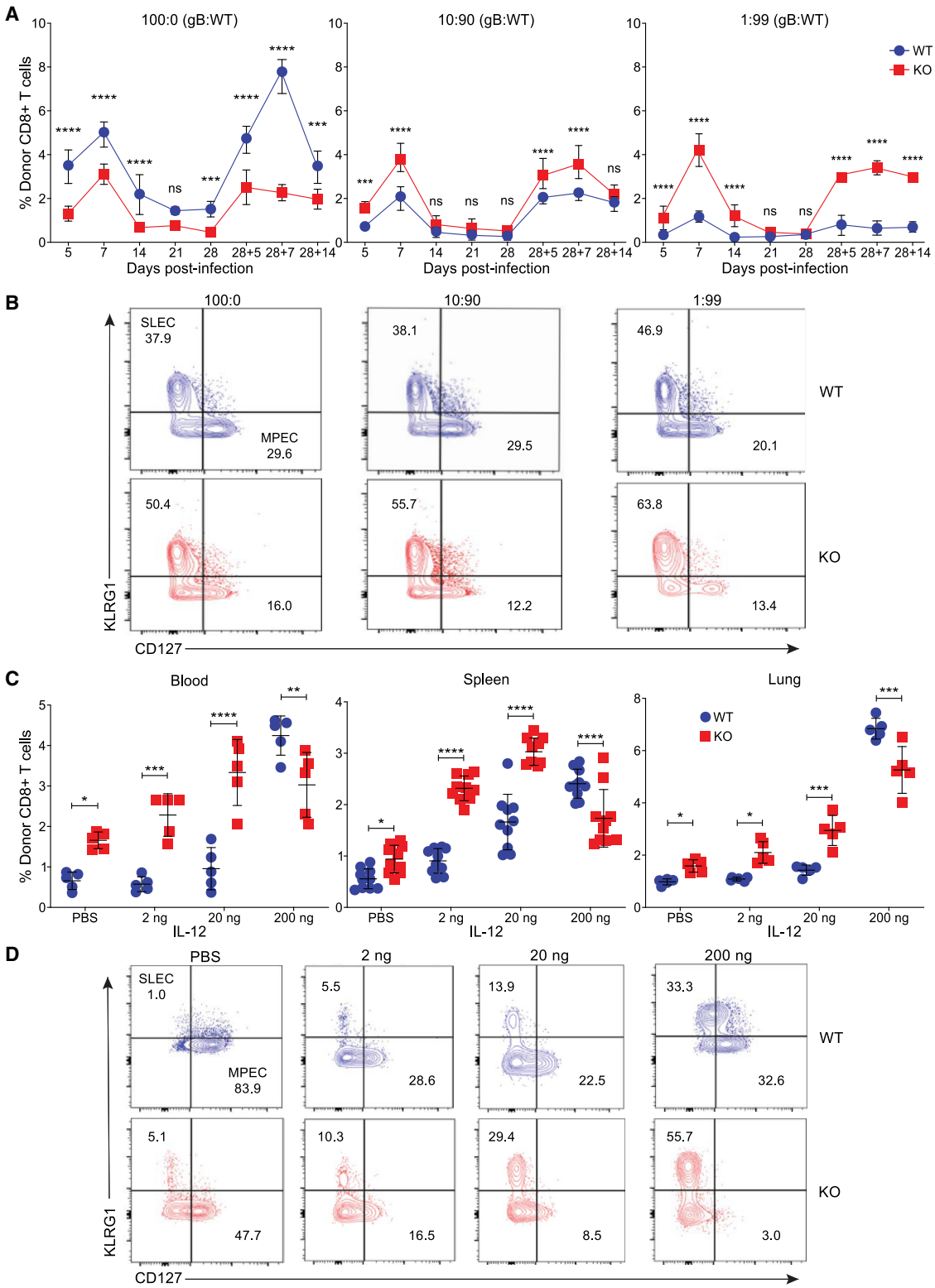

Figure 2. Loss of miR-29 lowers activation thresholds

(A) Kinetics of donor WT versus KO CD8+ T cell response from blood, with different ratios (indicated above plots) of LM-gB to WT LM, followed by secondary infection with LM-gB. Data represent mean ± SD of 2 experiments with 6-7 mice per group per experiment; 2-WAY ANOVA, ***p ≤ 0.001, ****p ≤ 0.0001.
(B) Representative contour plots of WT versus KO effector cell populations at 7 dpi as described in panel (A).

(legend continued on next page)

2015) (Figures 1B and S1B). These data imply roles for miR-29 in adult CD8+ T cells and suggest that low levels of miR-29 in neonates contribute to phenotypic differences between adult and neonatal cells.

To investigate the significance of miR-29 expression in adult CD8+ T cells, we performed adoptive single transfer experiments, comparing cells harboring floxed miR-29 from Cre+ and Cre- littermates (KO and WT, respectively) within congenically marked recipients, which we infected with a gBT-I recombinant vaccinia virus. Reduced miR-29 expression decreased the primary response somewhat and greatly impaired the memory recall response following reinfection (Figure 1C). When we examined the differentiation status of the effector pool at 7 days post-infection (dpi) (Joshi et al., 2007), loss of miR-29 increased the proportion of short-lived effector cells (SLECs) and reduced the proportion of memory precursor effector cells (MPECs) (Figures 1D and S1C). This MPEC skew was pathogen independent, observed in multiple organs, and throughout the primary and secondary responses (Figures 1D and S1C). Reduced miR-29 levels led to elevated secretion of inflammatory cytokines at 7 dpi, after gB peptide restimulation (Figure 1E), and after bystander activation (which is TCR independent; Kim and Shin, 2019) using IL-12 and IL-18 (Figure S1D). Moreover, loss of miR-29 decreased bacterial burden at the peak of the primary infection (Figure 1F) and, perhaps surprisingly, also after rechallenge infection (Figure S1E), despite the smaller magnitude of the recall response (Figure 1C). Increased pathogen clearance after reinfection may derive from an earlier peak of expansion following reinfection (Figure 1C) or possible changes in memory subsets. The changes caused by reduced miR-29 levels persisted in secondary effector cells, as seen by higher proportions of SLEC and pTem populations (Figure S1F). Furthermore, after rechallenge infection, loss of miR-29 resulted in downregulation of CD62L and upregulation of CXCR3, two markers of activation, for both KLRG1+ and KLRG1- effector subsets (Figure S1F). Thus, adult CD8+ T cells deficient in miR-29 resemble neonatal cells in terms of infection kinetics, rechallenge phenotype, effector cell populations, and cytokine profiles (Smith et al., 2014).

CD8+ T cells with high CX3CR1 levels typically differentiate into T effector memory (Tem) cells, whereas those with low levels are predisposed to become central memory (Tcm) cells (Gerlach et al., 2016). Reduced miR-29 levels increased CX3CR1 expression during primary infection (Figure S1G). Thus, we examined the memory repertoire at 35 dpi; CD8+ T cells with reduced miR-29 had an increased propensity to form effector-like subsets of memory T cells, including Tem and long-lived effector cells (LLECs) (Jameson and Masopust, 2018), with a reduction in long-lasting, tissue-specific and self-renewing memory cells (Figures 1G and S1H). These data indicate that loss of miR-29 in adult cells promotes a faster acting, more-differentiated memory repertoire with reduced self-renewal capacities. These altered proportions of memory cell subsets are reminiscent of those in neonates (Zhang et al., 2014).

Loss of miR-29 lowers activation thresholds

We hypothesized that miR-29 controls the activation threshold of naive cells. Thus, we used our conditional knockout model to test how loss of miR-29 impacted activation in single transfer experiments. We infected adult recipient mice with different ratios of WT and gB recombinant *Listeria monocytogenes* (LM-gB), and rechallenged with LM-gB. This strategy tested how loss of miR-29 alters sensitivity to low and high stimulus, while maintaining levels of inflammation. CD8+ T cells with reduced miR-29 required ~10- to 100-fold less stimulus to enable expansion throughout primary and secondary infections. However, under conditions of highest stimulation, KO cells exhibited a reduced response (Figure 2A). These results suggest that miR-29-deficient cells require minimal stimulation to induce a robust response yet are incapable of responding as effectively as WT cells under conditions of high stimulation. To confirm these results, we performed *in vitro* antigen titration experiments, which showed that miR-29-deficient cells proliferate faster than control cells when stimulated with low levels of gB peptide or by TCR stimulation (Figure S2A). Furthermore, miR-29-deficient cells require minimal stimulus to differentiate into SLECs and form few MPECs, regardless of the amount of stimulation during both the expansion and memory phases (Figures 2B, S2B, and S2C). This SLEC bias may derive from upregulation of Tbet and Eomes (Figure S2D), which promote effector cell differentiation (Jeker and Bluestone, 2013), and increased Blimp-1 (Figure S2E), which promotes SLEC formation (Rutishauser et al., 2009; Welsh, 2009).

After investigating antigen strength, we asked whether miR-29 affects the activation threshold initiated via IL-12, a cytokine important in CD8+ T cell differentiation (Joshi et al., 2007). Following transfer of gB-specific donor cells with reduced or normal levels of miR-29, we immunized recipient mice with dendritic cells loaded with gB peptide, and primed recipients with varying amounts of IL-12. Across multiple organs, CD8+ T cells with reduced miR-29 require minimal IL-12 stimulus to proliferate, but under high stimulus, their expansion plateaus at a lower point than Cre- control cells (Figure 2C). These results are supported by *in vitro* IL-12 stimulation assays (Figure S2A). Compared to their Cre- counterparts, the miR-29-deficient (KO; Cre+) cells required less IL-12 to differentiate into SLECs (Figures 2D and S2F), concomitant with dose-dependent upregulation of Blimp-1, Tbet, and Eomes (Figures S2G and S2H). These results suggest miR-29 helps establish normal activation thresholds, by both antigen and cytokine stimulation. In contrast, cells with less miR-29 exhibited a lower threshold, permitting rapid proliferation and differentiation upon activation at the expense of long-lived memory cell formation; phenotypes characteristic of neonates (Smith et al., 2014).

Impact of miR-29 on the naive CD8+ T cell transcriptome

CD8+ T cell naive populations are heterogeneous, and this complexity relates to compartmentalization of effector and

(C) Dot plots of WT versus KO donor cell proportions at 5 days post DC immunization with increased IL-12 priming versus negative PBS control in indicated organs. Data represent mean ± SD of 2 experiments with 5-10 mice per group per experiment; 2-WAY ANOVA, *$p \leq 0.05$, ***$p \leq 0.001$, ****$p \leq 0.0001$.
(D) Representative contour plots of WT versus KO effector cell populations at 5 days post DC immunization with IL-12 priming or PBS control.
See also Figure S2.

memory responses (Lee et al., 2013; Fink, 2013; van den Broek, Borghans and van Wijk, 2018; Kaech and Cui., 2012). We used single cell RNA-sequencing (scRNA-seq) to ask whether gene expression programs across the naive subpopulations are differentially impacted by miR-29. Using the 10x platform, we performed scRNA-seq on naive cells isolated from adult miR-29-deficient (Cre+; KO) and wild-type (Cre-; WT) littermates, and also from wild-type neonates, profiling an average of 4,880 cells per sample, and detecting a median of 2,058 genes per cell. There were 2,989 differentially expressed genes between WT adult and neonatal CD8+ T cells (Figure S3A), and 457 genes that differed between WT and KO adults (Figure S3B). Notably, multiple genes that drive effector differentiation were upregulated in the miR-29-deficient sample, including *Eomes* (Pearce et al., 2003) and *Cxcr3* (Kurachi et al., 2011), which are also expressed at high levels in neonates. UMAP (Uniform Manifold Approximation and Projection) analysis suggested subtle differences between samples, with multiple distinct clusters common to all samples (Figures 3A, 3B, and S3C). Nevertheless, the distribution of cells across clusters differed between samples (Figures 3C and S3D). When we examined the expression of miR-29 predicted targets, comparing each cluster individually between miR-29-deficient and WT adults, we found that all major clusters (96.7% of cells) exhibited significant loss of miR-29 regulation in Cre+ transcriptomes (KO; Figures 3C and S3E). To characterize the biological significance of the clusters, we examined established CD8+ T cell markers (Figure 3D). Expression of VM markers (*Cd44* and *Cd122*) was highest in clusters 3 and 7, and loss of miR-29 increased the proportion of cells within these clusters (Figure 3C). These results support flow cytometry analysis (Figure 1B), suggesting miR-29 promotes a TN fate. Similarly, *Eomes* and *Tbet* (*Tbx21*), which drive effector differentiation, were expressed highest in clusters 3 and 7. Collectively, these results show that loss of miR-29 in adults alters the transcriptome to promote neonatal-like features.

To investigate individual clusters, we performed enrichment analysis on marker genes of each cluster using ImmGen Consortium (IGC) gene sets, which describe expression signatures delineating naive CD8+ T cell expansion into precursor effector and subsequent memory cells (Best et al., 2013) (Figures 3E and S3F). Clusters 2, 5, and 6, which exhibited a decrease in cell proportions in miR-29-deficient as compared to control adult samples, were enriched for genes involved in late memory formation and depleted for those driving effector formation. Conversely, cluster 3, which was larger in the miR-29-deficient sample, was enriched for gene sets associated with effector cell function. These patterns were consistent when comparing unclustered adult control samples to either miR-29-deficient or neonatal samples (Figure S3G). These results suggest that loss of miR-29 in adults led to fewer naive cells with the potential to form long-lived memory cells. Finally, we examined enrichment across the IGC gene sets for differentially expressed genes in each cluster, comparing WT and KO adult transcriptomes (Figures 3F and S3H). Consistently, across the major clusters (1–5), loss of miR-29 led to an enrichment of gene sets involved in effector differentiation, particularly in cluster 3, which contained ~2-fold more cells than the control sample. Conversely, most major clusters in the adult control sample were enriched in gene sets associated with memory function (Figure 3F). These analyses demonstrate heterogeneity within the naive CD8+ T cell pool, and establish that miR-29 impacts the pool broadly, primarily by regulating the proportion of naive cells predisposed to differentiate toward memory or effector functions.

miR-29 reprograms naive neonatal CD8+ T cells to improve memory response

Our data indicate that normal miR-29 expression is necessary for CD8+ T cell memory functions in adults. Therefore, we asked whether ectopic miR-29 is sufficient to reprogram neonatal cells to mount an effective memory response. Current methods used to introduce genetic material into primary naive CD8+ T cells have major limitations: electroporation is inefficient and results in high death rates; lentiviral transduction requires prior activation of cells; and chemical transfection is inefficient and inadvertently activates cells. We devised a method of increasing miRNA levels in naive cells, based on delivery of RNAs to human and mouse cancer cells using extracellular vesicles (EVs) purified from human red blood cells as delivery vehicles (Usman et al., 2018). After purification, we loaded EVs with miR-29 or negative control (NC) miRNA mimics (Figure 4A) and confirmed delivery of miR-29 to naive neonatal cells by RT-qPCR (Figure 4B). We note that NC-loaded EVs had little impact on the naive cells, mediating no change in TN and VM proportions (Figures 4C and S4A).

EV-mediated delivery of miR-29 to neonatal cells decreased the proportion of VM cells (Figures 4C and S4A), and triggered downregulation of Tbet and Eomes (Figures 4D and S4B), phenotypes typical of adult cells. This is consistent with analysis of naive neonatal cells with natural variation in miR-29 levels (Figure S4C), demonstrating the robustness of EV-mediated delivery of miR-29. To examine the impact of miR-29 on response to infection, we performed adoptive transfers of neonatal cells treated with EVs and observed a striking increase in memory recall response after miR-29 delivery (Figure 4E). This change in response to infection is notable given that we introduced miR-29 in naive cells, with dilution of the mimic upon proliferation into effectors. While restimulated neonatal cells normally secrete more pro-inflammatory cytokines at the peak of infection compared to adult cells (Smith et al., 2014), production of IFNγ, GZMB and TNFα were decreased in response to miR-29 delivery to neonatal cells (Figures 4F and S4D). Consistent with increased cytokine production, expression of Tbet and Eomes at peak of infection was decreased (Figure S4E), transcription factors that promote formation of SLECs over MPECs (Joshi et al., 2007; Welsh, 2009). Indeed, the proportion of SLECs was reduced in neonatal cells treated with miR-29 accompanied by an increase in MPECs (Figures 4G and S4F). Thus, miR-29 overexpression in naive neonatal CD8+ T cells improves their response to reinfection, likely by modulating the ratio of effector cell types. Interestingly, this improvement persisted in the surface phenotype of secondary effectors after rechallenge infection, as judged by the decreased proportion of SLECs and pre-Tems, decreased CXCR3 expression, and increased CD62L expression (Figure S4G).

We examined the effect of miR-29 delivery to naive neonatal CD8+ T cells on the memory precursor populations generated during clonal expansion and on the memory repertoire after

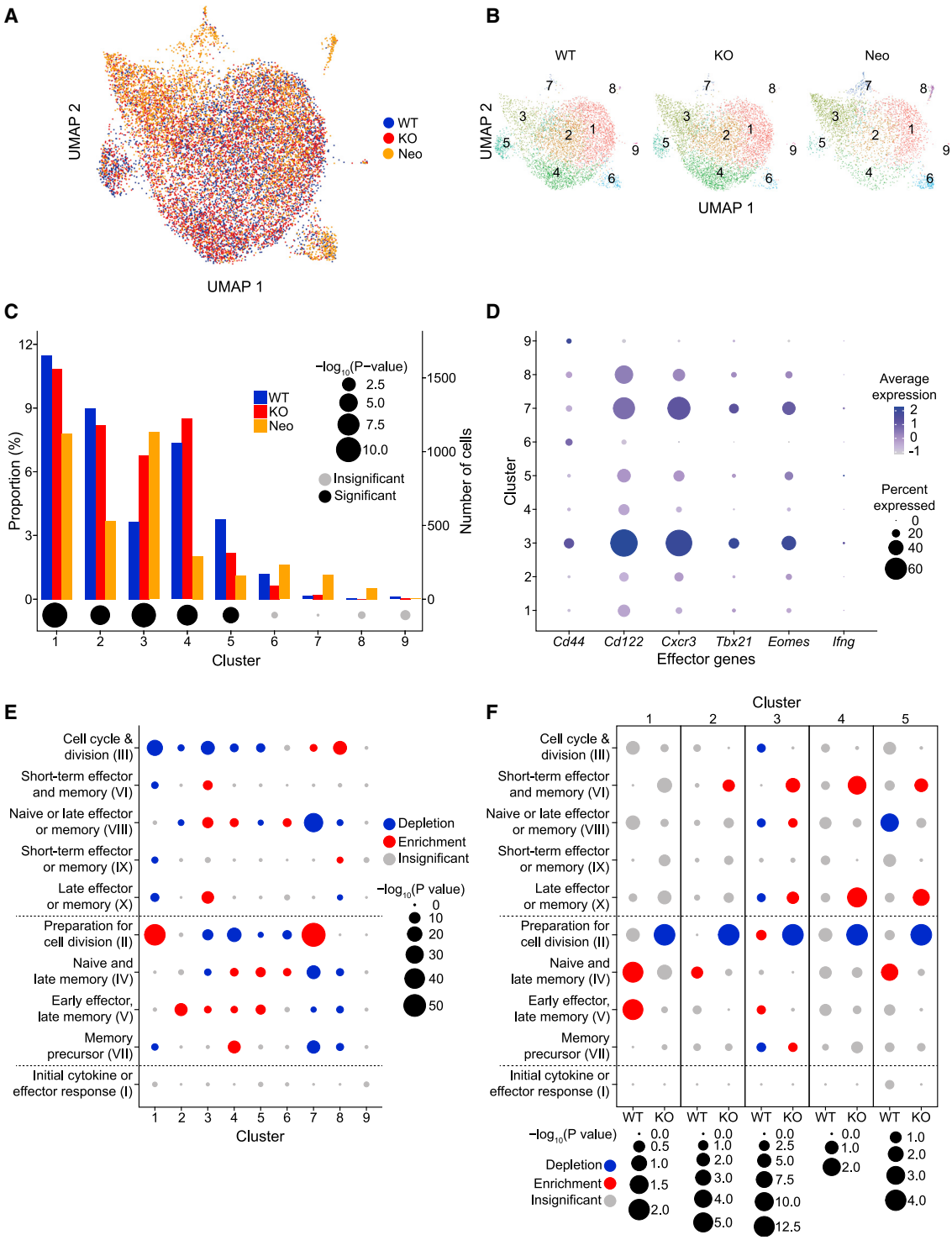

Figure 3. Analysis of naive transcriptomes by scRNA-seq

(A) scRNA-seq of WT and KO adult and neonatal (Neo) naive CD8+ T cells, visualized by UMAP.

(B) Individual UMAPs; as described in (A).

(C) Proportions of cells (y axis) for clusters (x axis; as identified in B); together with impact of miR-29 on predicted targets (x axis; p values denoted in legend).

(D) Expression of indicated genes (x axis), plotting percentage of cells expressing (denoted by circle size) and expression levels (color-coded) across clusters (y axis).

(E) Enrichment analysis for ImmGen gene sets (y axis) across clusters (x axis). Corrected p values denoted by circle size and color-coded (see legends).

(F) Enrichment analysis comparing WT and KO transcriptomes, for clusters 1 through 5; as described in (E).

See also Figure S3.

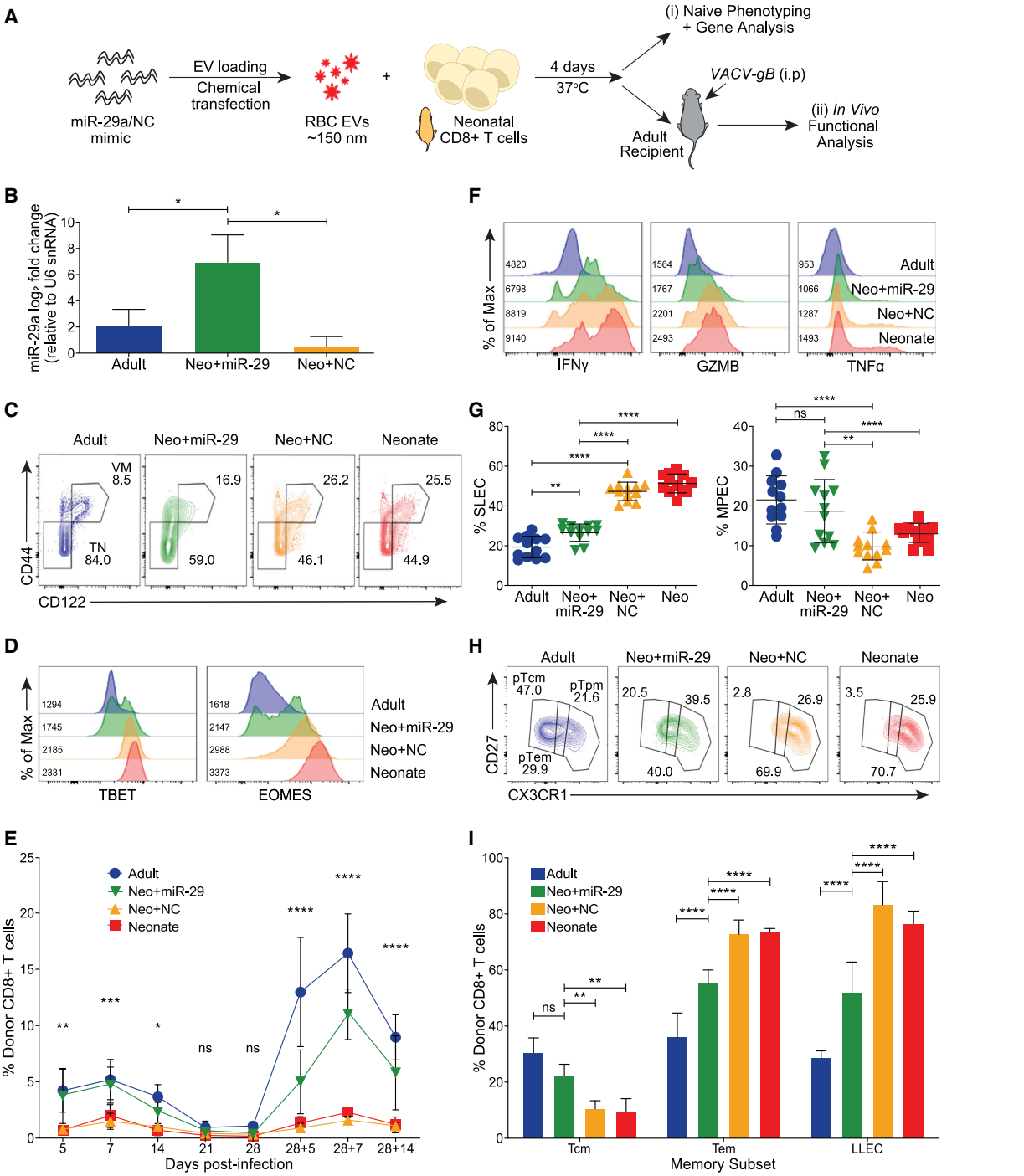

Figure 4. Induction of miR-29 in neonatal CD8+ T cells increases memory functions

(A) Experiment schematic.

(B) RT-qPCR quantification of miR-29a relative to U6 snRNA (y axis) from naive adult and EV-treated neonatal cells (x axis) delivering miR-29 or negative control (NC) mimics; data represent mean ± SD of 3 independent experiments with 2 mice per experiment; 2-WAY ANOVA, *p ≤ 0.05.

(C) Contour plots of TN and VM splenic CD8+ T cells from adult, neonate and EV-treated neonatal cells.

(D) Histograms of modal Tbet and Eomes expression from splenic naive cells.

(E) Kinetics of blood-derived donor cell proportion (y axis) through VACV-gB primary (5-28 dpi) and LM-gB secondary infections (x axis). Data represent mean ± SD of 2 independent experiments with 8-10 mice per group per experiment; 2-WAY ANOVA, *p ≤ 0.05, **p ≤ 0.01, ***p ≤ 0.001, ****p ≤ 0.0001.

(F) Histograms of modal cytokine expression after gB peptide restimulation of splenic donor CD8+ T cells at 7 dpi.

(legend continued on next page)

infection. Delivery of miR-29 decreased CX3CR1 expression, with an increase in precursor Tcm cells (preTcm) and decrease in precursor Tem cells (preTem) (Figures 4H and S4H). Moreover, at 35 dpi, we observed a decrease in both Tem and LLECs when cells were treated with miR-29 and an increase in Tcm and Trm proportions (Figures 4I and S4I). These results demonstrate that increasing miR-29 levels in naive neonatal CD8+ T cells is sufficient to form persistent, resident, canonical memory cells, approximating attributes of adult CD8+ T cells.

Impact of miR-29 on gene regulation in naive cells

Although miR-29 induction in naive neonatal CD8+ T cells led to an increased propensity to form memory cells, the identities of the underlying regulatory pathways were unclear. We performed RNA-seq to investigate changes in gene expression that result upon EV-mediated delivery of miR-29 to naive neonatal CD8+ T cells. Because of the extensive differences between TN and VM cells, we performed RNA-seq separately on each class of naive cell, including also naive cells from adults. Principal component analysis (PCA) revealed that PC1 correlated well with TN versus VM, as expected (Figure 5A). Notably, PC3 correlated with the adult-neonatal axis, and transcriptomes from neonatal cells treated with miR-29 moved toward adult transcriptomes, for both TN and VM samples but more pronounced in VM cells. PC2 and PC4, which were similar in scale to PC3, were more difficult to interpret (Figures S5A and S5B). Next, we performed enrichment analysis using the IGC gene sets (Figure 5B). In general, these analyses indicated that naive neonatal cells treated with miR-29 lose enrichment in multiple gene sets associated with effector status and are no longer depleted in memory gene sets. These changes were more evident for the VM cell comparisons. Taken together, these data indicate that raising levels of miR-29 in naive neonatal cells is sufficient to alter the transcriptome, inducing expression patterns more similar to adult cells.

To extend our analysis of regulatory changes induced by miR-29, we performed ATAC-seq on the same set of samples analyzed by RNA-seq, which allowed us to assess whether alterations to miR-29 levels in naive cells were sufficient to reprogram the chromatin landscape. PCA, using peaks detected by ATAC-seq as features, demonstrated clear partitioning of the different samples (Figure 5C). In contrast with the RNA-seq analysis, PC1 suggested an adult-neonatal axis, with PC2 suggesting the VM-TN axis. As before, exposure to miR-29 induced global changes, causing neonatal samples to resemble those of adults (Figure 5C). We performed enrichment analysis using IGC gene sets on the genes proximal to differentially accessible peaks, compared between control and miR-29-induced neonatal samples. Across multiple gene sets, genes close to peaks more accessible in miR-29-treated samples exhibited more adult-like signatures than the control neonatal samples (Figure S5C). To examine these changes in chromatin accessibility systematically, we performed k-means clustering (k = 6) on the ATAC-seq peaks, and then associated the peaks to the closest annotated gene. Next, we performed enrichment analysis on the clusters using the IGC gene sets (Figure 5D). There is a pronounced trend of miR-29-treated neonatal samples behaving as an intermediate between control neonatal and adult samples (Figure 5D, bottom). For example, cluster 4 contains ATAC-seq signatures that are highest for neonatal and lowest for adult samples, with intermediary signal from the miR-29-treated neonatal samples. This analysis indicated that cluster 4 is associated with effector gene sets, implying loss of accessible chromatin for such genes in response to miR-29. Cluster 1 also showed enrichment of effector gene sets, and the corresponding ATAC-seq signal is highest in the VM control neonatal samples and reduced in response to miR-29. Conversely, cluster 2 shows a depletion of effector gene sets, and the corresponding signal is highest in the adult samples and least accessible in neonates, with increased signal in the miR-29-treated neonatal samples. Thus, the chromatin landscape of naive neonatal CD8+ T cells loses signal at effector gene loci and gains signals at memory gene loci in response to miR-29; in both regards, these changes result in a landscape mimicking that of adult naive CD8+ T cells.

We next looked for enrichment of transcription factor (TF) binding motifs in the differently accessible chromatin regions. Runx-family-, Eomes-, and Tbet (Tbx21)-TF motifs are enriched in neonatal open chromatin regions, as expected for TFs involved in effector differentiation (Kaech and Cui, 2012; Best et al., 2013; Chen et al., 2018); miR-29 treatment reduced the extent of these enrichments. Similarly, motifs corresponding to the Foxo family and Pou/f family (*Oct1/2*), which are expressed in cells adopting an activated effector state (Hedrick et al., 2012; Shakya et al., 2011), were also most pronounced in neonatal samples, and elevated miR-29 reduced this enrichment (Figures 5E, 5F, S5D, S5E, S5F, and S5G; Table S1). KLF2, KLF4 and Sp1 motifs are enriched in adult but not neonatal samples; these factors contribute to maintenance of a nonproliferative state characteristic of adult naive CD8+ T cells (Weinreich et al., 2009; Yamada et al., 2009; Moskowitz et al., 2017). This suggests that TFs which restrain proliferation of adult naive cells are depleted in neonatal cells, lowering the proliferation threshold upon stimulation.

To examine TF binding induced by miR-29 more rigorously, we performed BaGFoot analysis, which identifies valleys or footprints caused by TF binding within accessible regions (Baek, Goldstein and Hager, 2017). This approach distinguishes between potentially active elements (accessible chromatin) from those that are implicated as active (footprinted). In VM cells, Eomes and Tbet (Tbx21) motifs are enriched in control neonatal cells compared to counterparts treated with miR-29; similar

(G) Quantification of SLEC (left) and MPEC (right) at 7 dpi from indicated samples based on KLRG1 versus CD127/IL7R. Data represent mean ± SD of 2 independent experiments with 6-7 mice per group per experiment. Otherwise as described in (E).
(H) Representative contour plots of pre-memory cell subsets across groups based on CD27 (y axis) and CX3CR1 (x axis) expression at 5 dpi.
(I) Bar graph quantification of CD8+ T cell memory subsets (x axis) Tcm (CD62L+ CD127+), Tem (CD62L- CD127+) and LLEC (KLRG1+ CD62L- CD43- CD27-) of donor cells at 35 dpi. Data represent mean ± SD of 2 independent experiments with 4-5 mice per group per experiment. Otherwise as described in (E). Representative gMFI values of respective groups indicated as a histogram inset.
See also Figure S4.

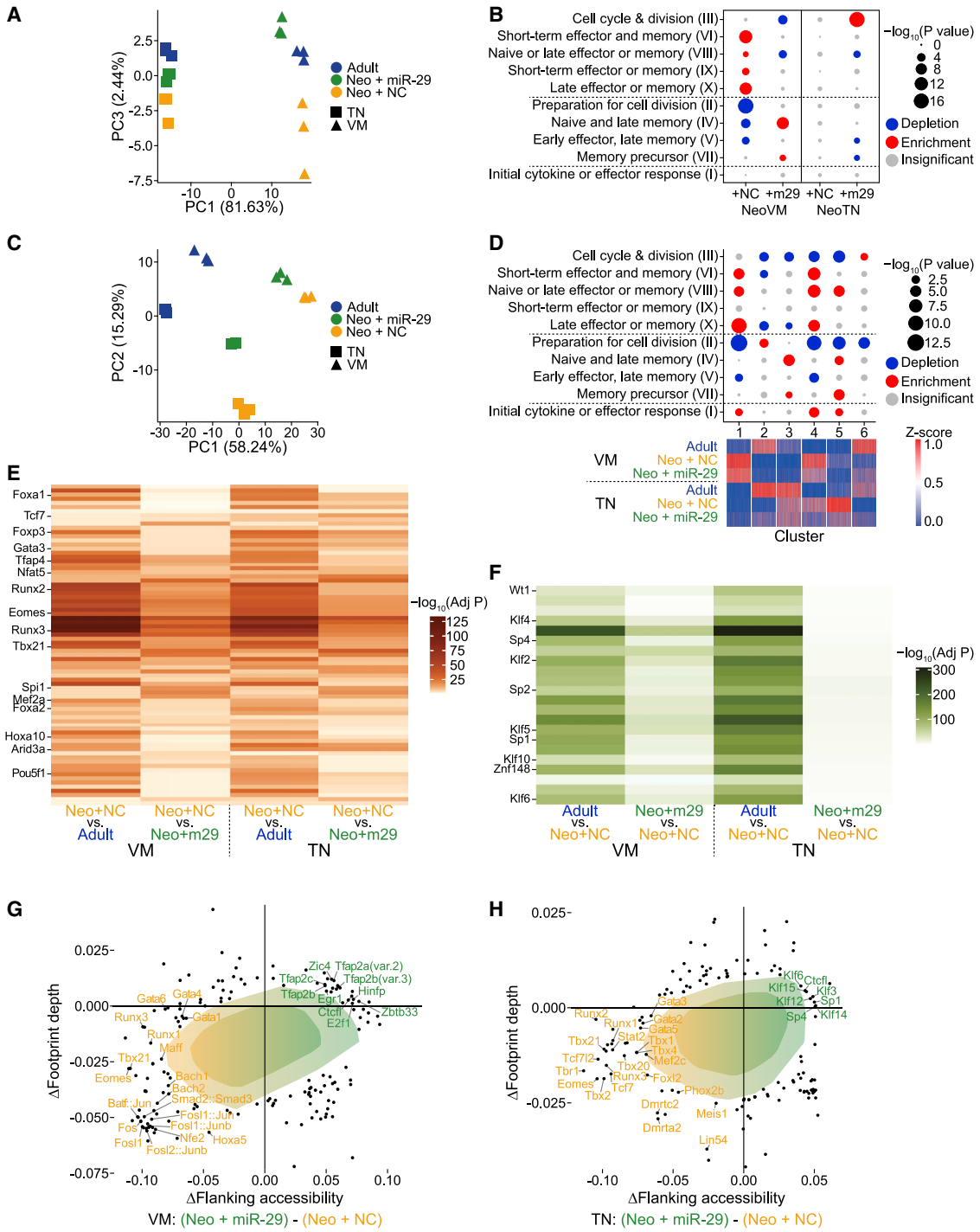

Figure 5. miR-29-mediated control of gene expression programs in CD8+ T cells

(A) PCA of RNA-seq from naive CD8+ T cells from adults and EV-treated neonates.

(B) Enrichment analysis with ImmGen gene sets on differentially expressed genes comparing EV-treated (NC versus miR-29) neonatal cells, for VM (left) and TN (right) transcriptomes. Circle sizes denote corrected p values, with enrichment and depletion color-coded (see legend).

(C) PCA of ATAC-seq from naive CD8+ T cells from adults and EV-treated neonates.

(D) Clustering of ATAC-seq peaks (bottom), and enrichment analyses per cluster (as described in B, top).

(E and F) Enrichment analyses of transcription factor (TF) binding motifs in differentially accessible chromatin regions, using ATAC-seq datasets from neonatal cells treated with control-EVs (Neo+NC), compared with indicated samples (x axis), plotting adjusted p values (color-coded, see inset legend) for motifs enriched in all four comparisons. Motifs with p values $\leq 10^{-320}$ plotted as 10^{-320}.

(legend continued on next page)

results were observed for Runx1 and AP-1 family members Fos and Jun, factors critical in the response to TCR stimulation (Jain et al., 1992) (Figures 5G and 5H; Table S2). Similar results were observed when comparing adult and neonatal samples (Figures S5H and S5I; Table S2). Interestingly, Bach, Smad and GATA motifs showed enrichment in control neonatal samples, which was diminished upon miR-29 treatment (Figures 5G, 5H, S5H, and S5I; Table S2); these TFs regulate effector states and differentiation in helper T cells (Richer, Lang and Butler, 2016; Malhotra and Kang., 2013; Lentjes et al., 2016). Overall, these analyses imply that differences in TF binding between adult and neonates can be partially recapitulated in neonatal cells by treating with miR-29.

Adjusting miR-29 levels in human CD8+ T cells

In human cells, miR-29 is also differentially expressed in an age-dependent manner (Wissink et al., 2015) (Figure S6A). We used our EV-delivery system to inhibit miR-29 in adult cells and supplement levels in umbilical cord blood-derived cells, in order to ask whether the age-dependent functions of miR-29 in mice exist also in humans (Figure 6A). MiR-29 levels were decreased significantly in naive human adult CD8+ T cells upon delivery of miR-29 inhibitor (ASO) (Figure 6B), resulting in upregulation of miR-29 targets (Figures 6C, S6B, and S6C). Similarly, miR-29 levels were modestly increased after delivery of miR-29 mimics to cord-derived naive cells (Figure 6D), resulting in more repression of miR-29 targets in response to increased, but still physiological, levels of miR-29 (Figures 6C, S6B, and S6C). Importantly, EV treatment alone did not significantly affect initial naive phenotypes after the 5-day EV incubation (Figure S6D).

Inhibition of miR-29 in naive adult cells was sufficient to increase expression of the activation markers CD69, CD25 and CD44, levels of effector cytokines, and proliferation (Figures 6E, S6E, and S6F). Thus, miR-29 modulation in human naive adult cells reprograms fundamental attributes of CD8+ T cells, resulting in a more cytotoxic state typical of newborns (Kwoczek et al., 2018; Jacks et al., 2018). Conversely, when we delivered miR-29 to naive human cord cells, levels of activation markers and effector cytokines were decreased, along with a reduction in proliferation (Figures 6F, S6E, and S6F). These results demonstrate that addition of miR-29 to human cord cells is sufficient to induce phenotypes characteristic of adults.

MiR-29-mediated gene regulation in human CD8+ T cells

To determine how miR-29 impacts gene regulation in human CD8+ T cells, we performed RNA-seq using naive human CD8+ T cells, in which we age-adjusted miR-29 levels using EVs. PCA showed a pronounced separation between adult and cord blood samples (PC1), with a clear difference between adults with and without miR-29 inhibition (PC3) and less pronounced differences between the two cord sample sets (Figure 7A). We note that PC2 appeared to reflect a batch effect and/or variation in expression between individuals (Figure S7A). We observed significant changes in expression of the miR-29 targets *TBX21* (*Tbet*) and *EOMES*, both as a function of age and upon modulation of miR-29 (Figure 7B). In addition, expression of many other effector genes changed upon miR-29 modulation, including *PRDM1* (*Blimp-1*), *CXCR3* and *CX3CR1* (Figure 7B).

To examine these changes more generally, we performed enrichment analysis using the IGC gene sets. Comparing the adult- and cord-derived transcriptomes from the control samples revealed that the cord-derived cells are enriched in gene sets associated with effector functions (Figure S7B). We next compared enrichments between the two sets of adult samples; inhibition of miR-29 increased enrichment of genes associated with cell cycling and division, and depleted genes associated with memory precursor status (Figure 7C). Comparisons between the two sets of cord-derived samples revealed that addition of miR-29 decreased enrichment in effector gene sets. Thus, in both humans and mice, age-adjusting miR-29 levels in naive cells alters the transcriptome extensively, driving long-lasting changes in downstream differentiated cells, and modulating the speed, strength, and longevity of response to infection.

DISCUSSION

Here, we establish a role for miR-29 in licensing adult CD8+ T cells toward memory fates, a conclusion supported by multiple lines of evidence. First, miR-29-deficient adult mice are unable to mount effective memory recall responses. We deleted the miR-29a/b-1 locus in only the $\alpha\beta$ T cell lineage, an important consideration as miR-29 has roles in hematopoietic progenitors and in non-immune lineages (Hilz et al., 2017; Mehta and Baltimore, 2016; Kriegel et al., 2012; Kwon et al., 2019). Second, miR-29 overexpression in naive neonatal mouse cells promotes adult-like phenotypes, increasing MPEC proportions and improving recall response. Finally, age-adjusting miR-29 levels in human or mouse naive CD8+ cells impacts gene expression programs; adult cells with reduced miR-29 levels show increased activity of genes associated with effector fates concomitant with a reduced activity of memory formation. Similarly, addition of miR-29 to naive neonatal cells is sufficient to bias expression programs toward those of adults. Thus, high miR-29 expression in adult CD8+ T cells is necessary for effective memory cell formation, and raising miR-29 levels in naive neonatal cells is sufficient to improve their memory response. Neonatal CD4+ T cells also express low levels of miR-29 (Yu et al., 2016) and fail to form memory cells (Zens et al., 2017); thus, our findings may also explain age-related differences in the CD4+ T cell response.

Age-related differences in T cell development in the thymus and fetal liver have been linked to regulation by Lin28 and the let-7 miRNA family, which is repressed by Lin28 (Pobezinsky et al., 2015; Yuan et al., 2012). These studies establish that in neonates, high levels of Lin28 and low let-7 program hematopoietic

(G and H) Bag plots analyzing footprints of TF motifs, compared between Neo+miR-29 and Neo+NC samples for VM (G) and TN (H) cells. Plotting flanking accessibility (x axis), and footprint depth (y axis).
See also Figure S5 and Tables S1–S2.

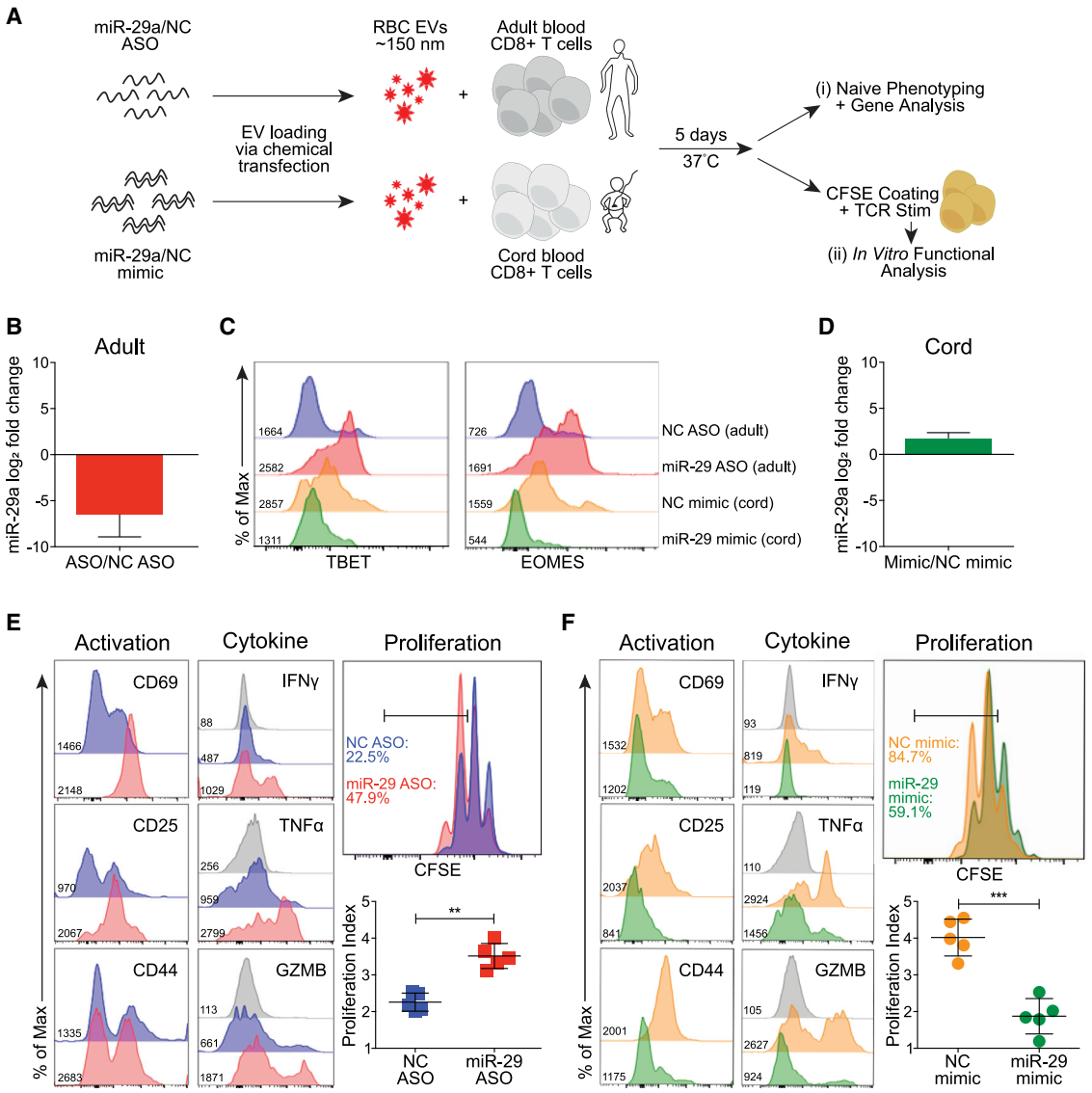

Figure 6. Reprogramming human CD8+ T cells by age-adjusting miR-29 levels

(A) Experiment schematic.

(B) RT-qPCR quantification of miR-29a (y axis) from naive adult cells treated with EVs loaded with miR-29 inhibitor (ASO) relative to negative control ASO (NC). Data represent mean ± SD of 3 independent experiments with 2-3 samples per experiment.

(C) Histograms of modal Tbet and Eomes expression, after EV-treatments of cord cells treated with miR-29 (mimic) or control (NC) oligonucleotides and adult cells treated with miR-29 inhibitor (ASO) or control (NC) oligonucleotides.

(D) RT-qPCR quantification of miR-29a (y axis) from naive cord cells treated with EVs loaded with miR-29 mimic relative to negative control mimic (NC). Data represent mean ± SD of 3 independent experiments with 2-3 samples per experiment.

(E) Histograms of flow measurements of activation markers, cytokines and CFSE (proliferation) from stimulated adult cells treated with EVs loaded with control (blue) or miR-29 ASO (red) or negative control (gray; no brefeldin A or monensin treatment). (Bottom right) Scatterplot of proliferation indices. Data represent mean ± SD of 2 experiments with 2-3 samples per experiment; unpaired Student's t test, **$p \leq 0.01$.

(F) Histograms, as described in (E), for cord-blood derived cells treated with EVs loaded with miR-29 (green) or negative control (orange) mimics. ***$p \leq 0.001$. Representative gMFI values of respective groups indicated as a histogram inset.

See also Figure S6.

stem cells and thymocytes to bias naive neonatal CD8+ T cells toward a VM phenotype, which is mediated, at least in part, by control of PLZF and IL-15. Thus, like miR-29, let-7 levels also contribute to establishing differences between the naive cells of adults and neonates, driving contrasting responses to infection. These results highlight the potential relationship between miR-29 and let-7/Lin-28, although it is unclear whether they are functioning in independent gene regulatory pathways, or whether both are key regulators in a unified pathway. Our data indicate that levels of miR-29 in naive CD8+ T cells are a critical

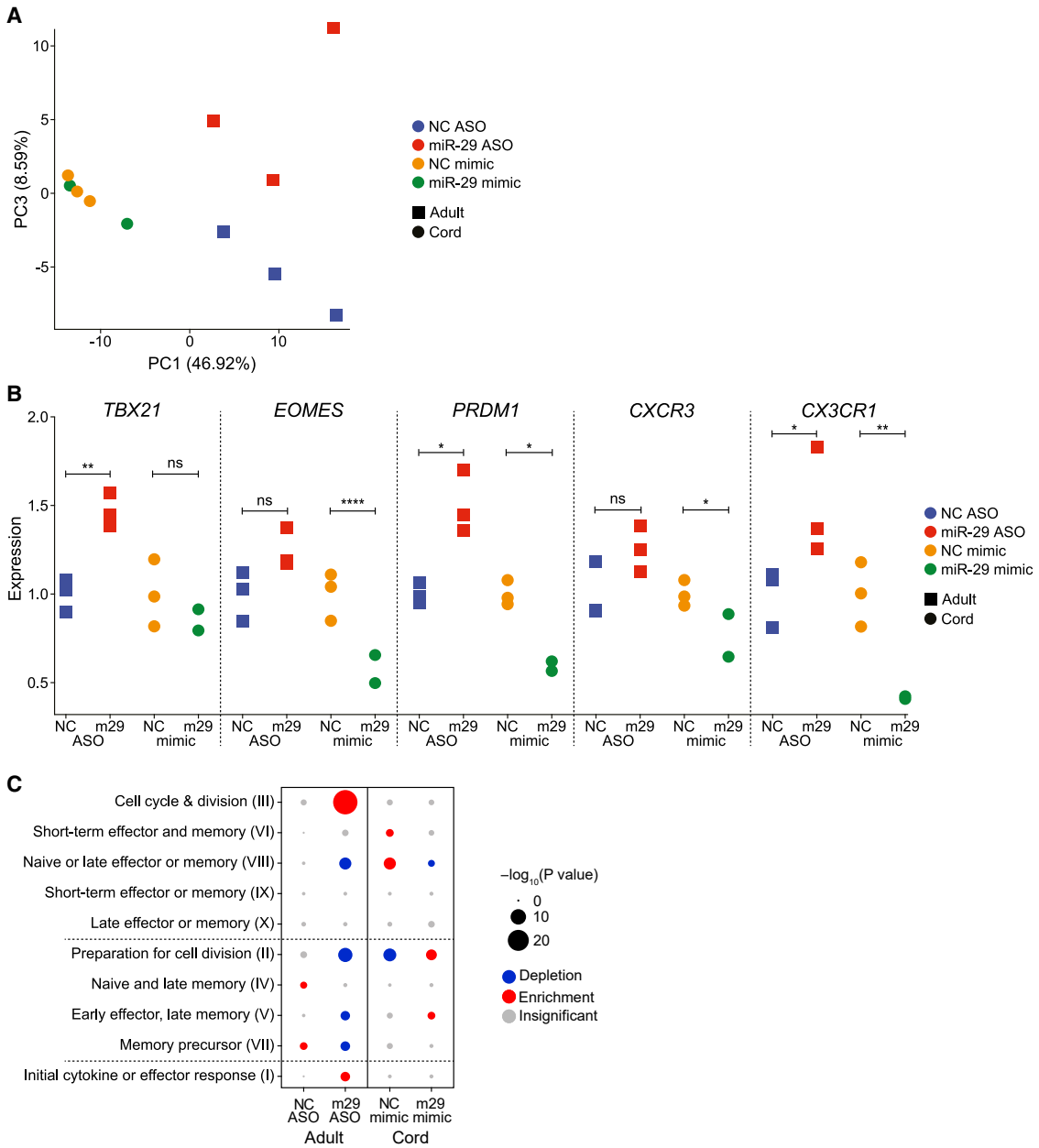

Figure 7. Human adult and cord CD8+ T cells can be transformed through manipulating the level of miR-29

(A) Principal component analysis of gene expression profiles for adult NC ASO, adult miR-29 ASO, cord NC ASO and cord miR-29 mimic samples, showing principal components 1 and 3.

(B) Expression of five genes relative to NC samples. Gene expression in adult NC and miR-29 ASO samples were normalized to mean expression of genes in the adult NC samples. Gene expression in cord NC and miR-29 mimic samples were normalized to mean expression of genes in the cord NC samples. p values were calculated by differential expression analysis; EdgeR, ****$p \leq 0.0001$, **$p \leq 0.01$, *$p \leq 0.05$

(C) Enrichment analysis for ImmGen gene sets on differentially expressed genes between adult NC and miR-29 ASO (left), cord NC and miR-29 mimic (right). Circle sizes denote corrected p values, with enrichment and depletion color coded (see legend).

See also Figure S7.

regulatory determinant, serving to modulate effector and memory responses, but how miR-29 affects let-7 regulation in progenitor cells remains unclear.

What is the teleological benefit of miR-29-mediated control of age-related differences in the CD8+ T cell response to infection? Our theory is that miR-29 levels control the activation 'set-point' in naive cells during different stages of life. In neonates, low miR-29 expression decreases the activation threshold, permitting a rapid proliferative response. While an enhanced capacity to proliferate may help neonates compensate for fewer CD8+ T cells,

the vigorous primary response comes at the expense of memory formation. Still, rapid protection may be advantageous during early stages of development, as immunological memory is unimportant if the host fails to survive. As the host ages and the naive T cell repertoire diversifies, increasing miR-29 expression raises the activation threshold, enabling a balanced response and retention of cells in the memory pool. Thus, miR-29 may act as a developmental switch, adjusting CD8+ T cell activation thresholds during different stages of life based upon the relative need to mount a rapid effector response versus generating long-lived memory cells.

Although miR-29 functions at multiple points during T cell development and after activation (Zhang and Bevan, 2010; Bronevetsky et al., 2013; Liston et al., 2012; Podshivalova and Salomon, 2013), a major point of consequential miR-29 activity is within naive cells. The long-lasting impact of miR-29 is conferred, at least in part, by changes in the chromatin landscape made in naive cells, which later impact downstream differentiation decisions. Presumably, certain enhancers whose accessibility is controlled by the miR-29 regulatory program only contribute to expression differences as naive CD8+ T cells activate and differentiate. This role for a miRNA, specifying cell fates before activation, expands upon the current dogma that miRNA regulation maintains the naive pool and also shapes the T cell response after activation (Wells, Pobezinskaya and Pobezinsky, 2020).

Currently, the field has proposed several models of T cell differentiation, including the 'decreasing potential hypothesis' (Kaech and Cui, 2012), but our data support the 'developmental programming pathway' model, whereby differently aged CD8+ T cells are programmed in the naive state. Our work suggests that miR-29 sculpts the regulatory program by targeting certain genes directly, in particular *Tbet* and *Eomes*, but many changes in gene expression, including *Cx3cr1, Cxcr3, Blimp-1, CD44,* and *IL2rb*, are downstream of these direct targets. Indeed, the extensive changes to the chromatin landscape documents the regulatory cascade initiated by miR-29. These alternatively programmed naive regulatory landscapes alter activation thresholds of CD8+ T cells, dictating their sensitivity toward antigenic and cytokine stimuli, thereby defining downstream effector states and memory cell lineages.

Methods to effectively manipulate CD8+ T cells while maintaining a naive state have been lacking. Viral transduction and transient delivery methods suffer from inefficient delivery and/or inadvertent cell activation. In addition, genetic approaches in mice are challenging for essential genes or those with pleiotropic phenotypes. We used extracellular vesicles (EVs) loaded *in vitro* to deliver miRNAs or miRNA inhibitors to naive primary human and mouse CD8+ T cells (Usman et al., 2018). Manipulation of miR-29 levels to alter memory cell differentiation may prove useful in vaccine design, autoimmunity treatment, and cancer therapeutics (Rupaimoole and Slack, 2017). Ultimately, the approach may have therapeutic applications (György et al., 2015), with potential relevance to engineered T cells, given that EVs can be loaded with a variety of biomolecules not limited to small RNAs.

Our work is notable for its potential to identify biomarkers that can predict vaccine success and infection outcomes in neonates. For example, relative miR-29 expression could provide an informative readout for the proportion of adult and young derived cells present at various stages of life, thus predicting the likelihood that a vaccine would result in generation of memory. Moreover, if baseline miR-29 expression predicts outcome, then more favorable vaccine outcomes could be achieved by manipulating miR-29 expression prior to immune challenge.

STAR★METHODS

Detailed methods are provided in the online version of this paper and include the following:

- KEY RESOURCES TABLE
- RESOURCE AVAILABILITY
  - Lead contact
  - Materials availability
  - Data and code availability
- EXPERIMENTAL MODEL AND SUBJECT DETAILS
  - Biological samples
  - Cell culture
- METHOD DETAILS
  - Tissue distribution and vascular staining
  - Flow cytometry
  - Adoptive single transfer experiments
  - Infections
  - Dendritic cell IL-12 immunization
  - PrimeFlow RNA Assay
  - Pathogen burden
  - *In vitro* mouse proliferation assay
  - *In vitro* mouse gB peptide restimulation
  - *In vitro* mouse bystander activation
  - PCR analysis of floxed miR-29ab1 locus
  - Quantitative RT-PCR (qRT-PCR)
  - RNA oligonucleotide sequences and modifications
  - Human RBC EV generation, purification and characterization
  - RBC-EV chemical transfection
  - *In vitro* EV nucleic acid treatment of naive mouse and human T cells
  - *In vitro* human TCR **stim, proliferation and cytokine** secretion assay
  - Mouse single cell RNA sequencing
  - Human CD8+ sorting for RNA-seq
  - Mouse CD8+ sorting for RNA-seq and ATAC-seq
  - Human/mouse RNA preparation and RNA sequencing
  - Mouse ATAC-seq nuclei prep, library preparation and sequencing
  - Single Cell RNA-seq analysis
  - miRNA targeting signature
  - Marker genes
  - Differential expression
  - Gene set analysis
  - ATAC-seq analysis
  - Principle Component Analysis (PCA)
  - Differential Accessibility
  - Clustering
  - Peak annotation

- Gene set analysis
- Transcription factor motifs
- Motif enrichment for transcription factor binding sites
- Transcription factor footprint identification
- Visualization
- RNA-seq analysis
- Differential expression and gene set analysis

- QUANTIFICATION AND STATISTICAL ANALYSIS

SUPPLEMENTAL INFORMATION

Supplemental information can be found online at https://doi.org/10.1016/j.celrep.2021.109969.

ACKNOWLEDGMENTS

We wish to thank the CARE staff at Cornell University (CU) for assistance with breeding mice and the Flow Cytometry Core at CU for their assistance. RNA-seq and ATAC-seq projects were coordinated by the CU TREx Facility and all sequencing was performed by the BRC Genomics Facility at CU. We would like to also acknowledge the support of the Cornell Nanoscale Science and Technology Facility under the NSF Grant ECCS-1542081 for use of equipment and experiment assistance. We wish to thank Dr. Gloria Pryhuber for human sample collection. This work was supported by NIH grant U01AI131348 awarded to B. Rudd, A. Grimson and D. Topham. C. Daly is supported by a fellowship from Boehringer Ingelheim Fonds.

AUTHOR CONTRIBUTIONS

All authors conceived and planned the experiments. K.Y.M., C.W.P.D., H.Z. and L.T.V. carried out the experiments, contributed to sample preparation and data analysis. N.L.S., R.P., M.T.N.L., A.G. and B.D.R. contributed to the interpretation of the results. K.Y.M., C.W.P.D., H.Z. and A.G. took the lead in writing the manuscript. All authors provided critical feedback and helped shape the research and manuscript.

DECLARATION OF INTERESTS

Authors Minh T. N. Le, Andrew Grimson, Brian D. Rudd, Kristel Yee Mon and Luyen Tien Vu, are co-inventors of a patent application entitled 'Delivery of nucleic acids into T cells' (US 63/000,468). Minh T.N. Le is a cofounder and advisor of Carmine Therapeutics, a company that develops EV-based therapeutics.

INCLUSION AND DIVERSITY

One or more of the authors of this paper self-identifies as an underrepresented ethnic minority in science.

Received: March 3, 2021
Revised: August 9, 2021
Accepted: October 19, 2021
Published: November 9, 2021

REFERENCES

Agarwal, V., Bell, G.W., Nam, J.-W., and Bartel, D.P. (2015). Predicting effective microRNA target sites in mammalian mRNAs. eLife *4*, e05005.

Baek, S., Goldstein, I., and Hager, G.L. (2017). Bivariate genomic footprinting detects changes in transcription factor activity. Cell Rep. *19*, 1710–1722.

Bailey, T.L., Boden, M., Buske, F.A., Frith, M., Grant, C.E., Clementi, L., Ren, J., Li, W.W., and Noble, W.S. (2009). MEME SUITE: Tools for motif discovery and searching. Nucleic Acids Res. *37*, W202–W208.

Bartel, D.P. (2009). MicroRNAs: Target recognition and regulatory functions. Cell *136*, 215–233.

Bartel, D.P. (2018). Metazoan MicroRNAs. Cell *173*, 20–51.

Basha, S., Surendran, N., and Pichichero, M. (2014). Immune responses in neonates. Expert Rev. Clin. Immunol. *10*, 1171–1184.

Best, J.A., Blair, D.A., Knell, J., Yang, E., Mayya, V., Doedens, A., Dustin, M.L., and Goldrath, A.W.; Immunological Genome Project Consortium (2013). Transcriptional insights into the CD8(+) T cell response to infection and memory T cell formation. Nat. Immunol. *14*, 404–412.

Bronevetsky, Y., Villarino, A.V., Eisley, C.J., Barbeau, R., Barczak, A.J., Heinz, G.A., Kremmer, E., Heissmeyer, V., McManus, M.T., Erle, D.J., et al. (2013). T cell activation induces proteasomal degradation of Argonaute and rapid remodeling of the microRNA repertoire. J. Exp. Med. *210*, 417–432.

Buenrostro, J.D., Wu, B., Chang, H.Y., and Greenleaf, W.J. (2015). ATAC-seq: A method for assaying chromatin accessibility genome-wide. Curr. Protoc. Mol. Biol. *109*, Published online January 5, 2015. https://doi.org/10.1002/0471142727.mb2129s109.

Butz, E.A., and Bevan, M.J. (1998). Massive expansion of antigen-specific CD8+ T cells during an acute virus infection. Immunity *8*, 167–175.

Chandiran, K., Lawlor, R., Pannuti, A., Perez, G.G., Srinivasan, J., Golde, T.E., Miele, L., Osborne, B.A., and Minter, L.M. (2018). Notch1 primes CD4 T cells for T helper type I differentiation through its early effects on miR-29. Mol. Immunol. *99*, 191–198.

Chen, Y., Zander, R., Khatun, A., Schauder, D.M., and Cui, W. (2018). Transcriptional and epigenetic regulation of effector and memory CD8 T cell differentiation. Front. Immunol. *9*, 2826.

Corces, M.R., Trevino, A.E., Hamilton, E.G., Greenside, P.G., Sinnott-Armstrong, N.A., Vesuna, S., Satpathy, A.T., Rubin, A.J., Montine, K.S., Wu, B., et al. (2017). An improved ATAC-seq protocol reduces background and enables interrogation of frozen tissues. Nat. Methods *14*, 959–962.

Dooley, J., Linterman, M.A., and Liston, A. (2013). MicroRNA regulation of T-cell development. Immunol. Rev. *253*, 53–64.

Fink, P.J. (2013). The biology of recent thymic emigrants. Annu. Rev. Immunol. *31*, 31–50.

Fornes, O., Castro-Mondragon, J.A., Khan, A., van der Lee, R., Zhang, X., Richmond, P.A., Modi, B.P., Correard, S., Gheorghe, M., Baranašić, D., et al. (2020). JASPAR 2020: update of the open-access database of transcription factor binding profiles. Nucleic Acids Res. *48* (*D1*), D87–D92.

Fulton, R.B., Hamilton, S.E., Xing, Y., Best, J.A., Goldrath, A.W., Hogquist, K.A., and Jameson, S.C. (2015). The TCR's sensitivity to self peptide-MHC dictates the ability of naive CD8(+) T cells to respond to foreign antigens. Nat. Immunol. *16*, 107–117.

Gerlach, C., Moseman, E.A., Loughhead, S.M., Alvarez, D., Zwijnenburg, A.J., Waanders, L., Garg, R., de la Torre, J.C., and von Andrian, U.H. (2016). The chemokine receptor CX3CR1 defines three antigen-experienced CD8 T cell subsets with distinct roles in immune surveillance and homeostasis. Immunity *45*, 1270–1284.

Gracias, D.T., Stelekati, E., Hope, J.L., Boesteanu, A.C., Doering, T.A., Norton, J., Mueller, Y.M., Fraietta, J.A., Wherry, E.J., Turner, M., and Katsikis, P.D. (2013). The microRNA miR-155 controls CD8(+) T cell responses by regulating interferon signaling. Nat. Immunol. *14*, 593–602.

György, B., Hung, M.E., Breakefield, X.O., and Leonard, J.N. (2015). Therapeutic applications of extracellular vesicles: clinical promise and open questions. Annu. Rev. Pharmacol. Toxicol. *55*, 439–464.

Hafemeister, C., and Satija, R. (2019). Normalization and variance stabilization of single-cell RNA-seq data using regularized negative binomial regression. Genome Biol. *20*, 296.

Hedrick, S.M., Hess Michelini, R., Doedens, A.L., Goldrath, A.W., and Stone, E.L. (2012). FOXO transcription factors throughout T cell biology. Nat. Rev. Immunol. *12*, 649–661.

Heinz, S., Benner, C., Spann, N., Bertolino, E., Lin, Y.C., Laslo, P., Cheng, J.X., Murre, C., Singh, H., and Glass, C.K. (2010). Simple combinations of lineage-determining transcription factors prime cis-regulatory elements required for macrophage and B cell identities. Mol. Cell *38*, 576–589.

Hilz, S., Fogarty, E.A., Modzelewski, A.J., Cohen, P.E., and Grimson, A. (2017). Transcriptome profiling of the developing male germ line identifies the miR-29 family as a global regulator during meiosis. RNA Biol. *14*, 219–235.

Jacks, R.D., Keller, T.J., Nelson, A., Nishimura, M.I., White, P., and Iwashima, M. (2018). Cell intrinsic characteristics of human cord blood naïve CD4T cells. Immunol. Lett. *193*, 51–57.

Jain, J., McCaffrey, P.G., Valge-Archer, V.E., and Rao, A. (1992). Nuclear factor of activated T cells contains Fos and Jun. Nature *356*, 801–804.

Jameson, S.C., and Masopust, D. (2018). Understanding subset diversity in T cell memory. Immunity *48*, 214–226.

Jeker, L.T., and Bluestone, J.A. (2013). MicroRNA regulation of T-cell differentiation and function. Immunol. Rev. *253*, 65–81.

Joshi, N.S., Cui, W., Chandele, A., Lee, H.K., Urso, D.R., Hagman, J., Gapin, L., and Kaech, S.M. (2007). Inflammation directs memory precursor and short-lived effector CD8(+) T cell fates via the graded expression of T-bet transcription factor. Immunity *27*, 281–295.

Kaech, S.M., and Cui, W. (2012). Transcriptional control of effector and memory CD8+ T cell differentiation. Nat. Rev. Immunol. *12*, 749–761.

Kim, T.-S., and Shin, E.-C. (2019). The activation of bystander $CD8^+$ T cells and their roles in viral infection. Exp. Mol. Med. *51*, 1–9.

Kim, D., Paggi, J.M., Park, C., Bennett, C., and Salzberg, S.L. (2019). Graph-based genome alignment and genotyping with HISAT2 and HISAT-genotype. Nat. Biotechnol. *37*, 907–915.

Korsunsky, I., Millard, N., Fan, J., Slowikowski, K., Zhang, F., Wei, K., Baglaenko, Y., Brenner, M., Loh, P.R., and Raychaudhuri, S. (2019). Fast, sensitive and accurate integration of single-cell data with harmony. Nat. Methods *16*, 1289–1296.

Kriegel, A.J., Liu, Y., Fang, Y., Ding, X., and Liang, M. (2012). The miR-29 family: genomics, cell biology, and relevance to renal and cardiovascular injury. Physiol. Genomics *44*, 237–244.

Kroesen, B.-J., Teteloshvili, N., Smigielska-Czepiel, K., Brouwer, E., Boots, A.M.H., van den Berg, A., and Kluiver, J. (2015). Immuno-miRs: critical regulators of T-cell development, function and ageing. Immunology *144*, 1–10.

Kurachi, M., Kurachi, J., Suenaga, F., Tsukui, T., Abe, J., Ueha, S., Tomura, M., Sugihara, K., Takamura, S., Kakimi, K., and Matsushima, K. (2011). Chemokine receptor CXCR3 facilitates CD8(+) T cell differentiation into short-lived effector cells leading to memory degeneration. J. Exp. Med. *208*, 1605–1620.

Kwoczek, J., Riese, S.B., Tischer, S., Bak, S., Lahrberg, J., Oelke, M., Maul, H., Blasczyk, R., Sauer, M., and Eiz-Vesper, B. (2018). Cord blood-derived T cells allow the generation of a more naïve tumor-reactive cytotoxic T-cell phenotype. Transfusion *58*, 88–99.

Kwon, J.J., Factora, T.D., Dey, S., and Kota, J. (2019). A systematic review of miR-29 in Cancer. Mol. Ther. Oncolytics *12*, 173–194.

Lee, J.-Y., Hamilton, S.E., Akue, A.D., Hogquist, K.A., and Jameson, S.C. (2013). Virtual memory CD8 T cells display unique functional properties. Proc. Natl. Acad. Sci. USA *110*, 13498–13503.

Lentjes, M.H., Niessen, H.E., Akiyama, Y., de Bruïne, A.P., Melotte, V., and van Engeland, M. (2016). The emerging role of GATA transcription factors in development and disease. Expert Rev. Mol. Med. *18*, e3.

Li, Q., Brown, J.B., Huang, H., and Bickel, P.J. (2011). Measuring reproducibility of high- throughput experiments. Ann. Appl. Stat. *5*, 1752–1779.

Liang, Y., Pan, H.-F., and Ye, D.-Q. (2015). microRNAs function in CD8+T cell biology. J. Leukoc. Biol. *97*, 487–497.

Liao, Y., Smyth, G.K., and Shi, W. (2014). featureCounts: an efficient general purpose program for assigning sequence reads to genomic features. Bioinformatics *30*, 923–930.

Liston, A., Papadopoulou, A.S., Danso-Abeam, D., and Dooley, J. (2012). MicroRNA-29 in the adaptive immune system: setting the threshold. Cell. Mol. Life Sci. *69*, 3533–3541.

Love, M.I., Huber, W., and Anders, S. (2014). Moderated estimation of fold change and dispersion for RNA-seq data with DESeq2. Genome Biol. *15*, 550.

Ma, F., Xu, S., Liu, X., Zhang, Q., Xu, X., Liu, M., Hua, M., Li, N., Yao, H., and Cao, X. (2011). The microRNA miR-29 controls innate and adaptive immune responses to intracellular bacterial infection by targeting interferon-γ. Nat. Immunol. *12*, 861–869.

Malhotra, N., and Kang, J. (2013). SMAD regulatory networks construct a balanced immune system. Immunology *139*, 1–10.

McCarthy, D.J., Chen, Y., and Smyth, G.K. (2012). Differential expression analysis of multifactor RNA-Seq experiments with respect to biological variation. Nucleic Acids Res. *40*, 4288–4297.

McLeay, R.C., and Bailey, T.L. (2010). Motif enrichment analysis: a unified framework and an evaluation on ChIP data. BMC Bioinformatics *11*, 165.

Mehta, A., and Baltimore, D. (2016). MicroRNAs as regulatory elements in immune system logic. Nat. Rev. Immunol. *16*, 279–294.

Moskowitz, D.M., Zhang, D.W., Hu, B., Le Saux, S., Yanes, R.E., Ye, Z., Buenrostro, J.D., Weyand, C.M., Greenleaf, W.J., and Goronzy, J.J. (2017). Epigenomics of human CD8 T cell differentiation and aging. Sci. Immunol. *2*, eaag0192.

Mueller, S.N., Heath, W., McLain, J.D., Carbone, F.R., and Jones, C.M. (2002). Characterization of two TCR transgenic mouse lines specific for herpes simplex virus. Immunol. Cell Biol. *80*, 156–163.

Muljo, S.A., Ansel, K.M., Kanellopoulou, C., Livingston, D.M., Rao, A., and Rajewsky, K. (2005). Aberrant T cell differentiation in the absence of Dicer. J. Exp. Med. *202*, 261–269.

O'Connell, R.M., Rao, D.S., Chaudhuri, A.A., and Baltimore, D. (2010). Physiological and pathological roles for microRNAs in the immune system. Nat. Rev. Immunol. *10*, 111–122.

Orr, M.T., Orgun, N.N., Wilson, C.B., and Way, S.S. (2007). Cutting edge: recombinant Listeria monocytogenes expressing a single immune-dominant peptide confers protective immunity to herpes simplex virus-1 infection. J. Immunol. *178*, 4731–4735.

Pearce, E.L., Mullen, A.C., Martins, G.A., Krawczyk, C.M., Hutchins, A.S., Zediak, V.P., Banica, M., DiCioccio, C.B., Gross, D.A., Mao, C.A., et al. (2003). Control of effector CD8+ T cell function by the transcription factor Eomesodermin. Science *302*, 1041–1043.

Philbin, V.J., and Levy, O. (2009). Developmental biology of the innate immune response: implications for neonatal and infant vaccine development. Pediatr. Res. *65*, 98R–105R.

Pobezinsky, L.A., Etzensperger, R., Jeurling, S., Alag, A., Kadakia, T., McCaughtry, T.M., Kimura, M.Y., Sharrow, S.O., Guinter, T.I., Feigenbaum, L., and Singer, A. (2015). Let-7 microRNAs target the lineage-specific transcription factor PLZF to regulate terminal NKT cell differentiation and effector function. Nat. Immunol. *16*, 517–524.

Podshivalova, K., and Salomon, D.R. (2013). MicroRNA regulation of T-lymphocyte immunity: modulation of molecular networks responsible for T-cell activation, differentiation, and development. Crit. Rev. Immunol. *33*, 435–476.

Ramírez, F., Ryan, D.P., Grüning, B., Bhardwaj, V., Kilpert, F., Richter, A.S., Heyne, S., Dündar, F., and Manke, T. (2016). deepTools2: a next generation web server for deep-sequencing data analysis. Nucleic Acids Res. *44* (*W1*), W160–W165.

Reynaldi, A., Smith, N.L., Schlub, T.E., Venturi, V., Rudd, B.D., and Davenport, M.P. (2016). Modeling the dynamics of neonatal $CD8^+$ T-cell responses. Immunol. Cell Biol. *94*, 838–848.

Richer, M.J., Lang, M.L., and Butler, N.S. (2016). T cell fates zipped up: how the Bach2 basic leucine zipper transcriptional repressor directs T cell differentiation and function. J. Immunol. *197*, 1009–1015.

Robinson, M.D., McCarthy, D.J., and Smyth, G.K. (2010). edgeR: A bioconductor package for differential expression analysis of digital gene expression data. Bioinformatics *26*, 139–140.

Rudd, B.D. (2020). Neonatal T Cells: A Reinterpretation. Annu. Rev. Immunol. *38*, 229–247.

Rudd, B.D., Venturi, V., Davenport, M.P., and Nikolich-Žugich, J. (2011). Evolution of the antigen-specific CD8+ TCR repertoire across the life

span: evidence for clonal homogenization of the old TCR repertoire. J. Immunol. *186*, 2056–2064.

Rupaimoole, R., and Slack, F.J. (2017). MicroRNA therapeutics: towards a new era for the management of cancer and other diseases. Nat. Rev. Drug Discov. *16*, 203–222.

Rutishauser, R.L., Martins, G.A., Kalachikov, S., Chandele, A., Parish, I.A., Meffre, E., Jacob, J., Calame, K., and Kaech, S.M. (2009). Transcriptional repressor Blimp-1 promotes CD8(+) T cell terminal differentiation and represses the acquisition of central memory T cell properties. Immunity *31*, 296–308.

Shakya, A., Kang, J., Chumley, J., Williams, M.A., and Tantin, D. (2011). Oct1 is a switchable, bipotential stabilizer of repressed and inducible transcriptional states. J. Biol. Chem. *286*, 450–459.

Smith, K.M., Guerau-de-Arellano, M., Costinean, S., Williams, J.L., Bottoni, A., Mavrikis Cox, G., Satoskar, A.R., Croce, C.M., Racke, M.K., Lovett-Racke, A.E., and Whitacre, C.C. (2012). miR-29ab1 deficiency identifies a negative feedback loop controlling Th1 bias that is dysregulated in multiple sclerosis. J. Immunol. *189*, 1567–1576.

Smith, N.L., Wissink, E., Wang, J., Pinello, J.F., Davenport, M.P., Grimson, A., and Rudd, B.D. (2014). Rapid proliferation and differentiation impairs the development of memory CD8+ T cells in early life. J. Immunol. *193*, 177–184.

Smith, N.L., Wissink, E.M., Grimson, A., and Rudd, B.D. (2015). miR-150 regulates differentiation and cytolytic effector function in CD8+ T cells. Sci. Rep. *5*, 16399.

Smith, N.L., Patel, R.K., Reynaldi, A., Grenier, J.K., Wang, J., Watson, N.B., Nzingha, K., Yee Mon, K.J., Peng, S.A., Grimson, A., et al. (2018). Developmental origin governs $CD8^+$ T cell fate decisions during infection. Cell *174*, 117–130.e14.

Smithey, M.J., Brandt, S., Freitag, N.E., Higgins, D.E., and Bouwer, H.G.A. (2008). Stimulation of enhanced CD8 T cell responses following immunization with a hyper-antigen secreting intracytosolic bacterial pathogen. J. Immunol. *180*, 3406–3416.

Steiner, D.F., Thomas, M.F., Hu, J.K., Yang, Z., Babiarz, J.E., Allen, C.D., Matloubian, M., Blelloch, R., and Ansel, K.M. (2011). MicroRNA-29 regulates T-box transcription factors and interferon-γ production in helper T cells. Immunity *35*, 169–181.

Stuart, T., Butler, A., Hoffman, P., Hafemeister, C., Papalexi, E., Mauck, W.M., 3rd, Hao, Y., Stoeckius, M., Smibert, P., and Satija, R. (2019). Comprehensive integration of single-cell data. Cell *177*, 1888–1902.e21.

Tabilas, C., Wang, J., Liu, X., Locasale, J.W., Smith, N.L., and Rudd, B.D. (2019). Cutting edge: elevated glycolytic metabolism limits the formation of memory $CD8^+$ T Cells in Early Life. J. Immunol. *203*, 2571–2576.

Usman, W.M., Pham, T.C., Kwok, Y.Y., Vu, L.T., Ma, V., Peng, B., Chan, Y.S., Wei, L., Chin, S.M., Azad, A., et al. (2018). Efficient RNA drug delivery using red blood cell extracellular vesicles. Nat. Commun. *9*, Published online June 15, 2018. https://doi.org/10.1038/s41467-018-04791-8.

van den Broek, T., Borghans, J.A.M., and van Wijk, F. (2018). The full spectrum of human naive T cells. Nat. Rev. Immunol. *18*, 363–373.

Wang, J., Wissink, E.M., Watson, N.B., Smith, N.L., Grimson, A., and Rudd, B.D. (2016). Fetal and adult progenitors give rise to unique populations of CD8+ T cells. Blood *128*, 3073–3082.

Weinreich, M.A., Takada, K., Skon, C., Reiner, S.L., Jameson, S.C., and Hogquist, K.A. (2009). KLF2 transcription-factor deficiency in T cells results in unrestrained cytokine production and upregulation of bystander chemokine receptors. Immunity *31*, 122–130.

Wells, A.C., Pobezinskaya, E.L., and Pobezinsky, L.A. (2020). Non-coding RNAs in CD8 T cell biology. Mol. Immunol. *120*, 67–73.

Welsh, R.M. (2009). Blimp hovers over T cell immunity. Immunity *31*, 178–180.

Whitmire, J.K., Tan, J.T., and Whitton, J.L. (2005). Interferon-γ acts directly on CD8+ T cells to increase their abundance during virus infection. J. Exp. Med. *201*, 1053–1059.

Wissink, E.M., Smith, N.L., Spektor, R., Rudd, B.D., and Grimson, A. (2015). MicroRNAs and their targets are differentially regulated in adult and neonatal mouse CD8+ T cells. Genetics *201*, 1017–1030.

Wu, H., Neilson, J.R., Kumar, P., Manocha, M., Shankar, P., Sharp, P.A., and Manjunath, N. (2007). miRNA profiling of naïve, effector and memory CD8 T cells. PLoS ONE *2*, e1020.

Wu, T., Wieland, A., Araki, K., Davis, C.W., Ye, L., Hale, J.S., and Ahmed, R. (2012). Temporal expression of microRNA cluster miR-17-92 regulates effector and memory CD8+ T-cell differentiation. Proc. Natl. Acad. Sci. USA *109*, 9965–9970.

Yamada, T., Park, C.S., Mamonkin, M., and Lacorazza, H.D. (2009). Transcription factor ELF4 controls the proliferation and homing of CD8+ T cells via the Krüppel-like factors KLF4 and KLF2. Nat. Immunol. *10*, 618–626.

Yang, L., Boldin, M.P., Yu, Y., Liu, C.S., Ea, C.-K., Ramakrishnan, P., Taganov, K.D., Zhao, J.L., and Baltimore, D. (2012). miR-146a controls the resolution of T cell responses in mice. J. Exp. Med. *209*, 1655–1670.

Yu, H.-R., Hsu, T.-Y., Huang, H.-C., Kuo, H.-C., Li, S.-C., Yang, K.D., and Hsieh, K.-S. (2016). Comparison of the functional microRNA expression in immune cell subsets of neonates and adults. Front. Immunol. *7*, 615.

Yu, J.C., Khodadadi, H., Malik, A., Davidson, B., Salles, É.D.S.L., Bhatia, J., Hale, V.L., and Baban, B. (2018). Innate immunity of neonates and infants. Front. Immunol. *9*, 1759.

Yuan, J., Nguyen, C.K., Liu, X., Kanellopoulou, C., and Muljo, S.A. (2012). Lin28b reprograms adult bone marrow hematopoietic progenitors to mediate fetal-like lymphopoiesis. Science *335*, 1195–1200.

Zens, K.D., Chen, J.K., Guyer, R.S., Wu, F.L., Cvetkovski, F., Miron, M., and Farber, D.L. (2017). Reduced generation of lung tissue-resident memory T cells during infancy. J. Exp. Med. *214*, 2915–2932.

Zhang, N., and Bevan, M.J. (2010). Dicer controls CD8+ T-cell activation, migration, and survival. Proc. Natl. Acad. Sci. USA *107*, 21629–21634.

Zhang, Y., Liu, T., Meyer, C.A., Eeckhoute, J., Johnson, D.S., Bernstein, B.E., Nusbaum, C., Myers, R.M., Brown, M., Li, W., and Liu, X.S. (2008). Model-based analysis of ChIP-Seq (MACS). Genome Biol. *9*, R137.

Zhang, X., Mozeleski, B., Lemoine, S., Dériaud, E., Lim, A., Zhivaki, D., Azria, E., Le Ray, C., Roguet, G., Launay, O., et al. (2014). CD4 T cells with effector memory phenotype and function develop in the sterile environment of the fetus. Sci. Transl. Med. *6*, 238ra72.

Zhang, T., Zhang, Z., Li, F., Ping, Y., Qin, G., Zhang, C., and Zhang, Y. (2018). miR-143 regulates memory T cell differentiation by reprogramming T cell metabolism. J. Immunol. *201*, 2165–2175.

STAR★METHODS

KEY RESOURCES TABLE

Reagent or resource	Source	Identifier
Antibodies		
Anti-mouse CD8a	BD Biosciences	Cat# 563786; RRID: AB_2732919
anti-mouse CD62L	BD Biosciences	Cat# 560516; RRID: AB_1645257
anti-mouse CD45.1	Thermo Fisher Scientific	Cat#17-0453-82; RRID: AB_469398
anti-mouse CD45.2	Thermo Fisher Scientific	Cat#47-0454-82; RRID: AB_1272175
anti-mouse CD4	Thermo Fisher Scientific	Cat# 48-0042-82; RRID: AB_1272194)
anti-mouse CD127	Thermo Fisher Scientific	Cat# 12-1271-82; RRID: AB_465844
anti-mouse CD27	Thermo Fisher Scientific	Cat# 11-0271-81; RRID: AB_465000
anti-mouse KLRG1	Thermo Fisher Scientific	Cat#46-5893-82; RRID: AB_10670282
anti-mouse CD25	Thermo Fisher Scientific	Cat#17-0251-82; RRID: AB_469366
anti-mouse/human CD44	Thermo Fisher Scientific	Cat# 17-0441-82; RRID: AB_46939
anti-mouse Ly-6C	Thermo Fisher Scientific	Cat#47-5932-82; RRID: AB_2573992
anti-mouse CD122	Thermo Fisher Scientific	Cat#46-1222-82; RRID: AB_11064442
anti-mouse CD8b	Biologend	Cat# 126612; RRID: AB_2075777
anti-mouse CX3CR1	Biolegend	Cat# 149008, RRID: AB_2564492
anti-mouse CXCR3	Biolegend	Cat# 126505; RRID: AB_1027656
anti-mouse CD43	Biolegend	Cat# 143206; RRID: AB_11124719
anti-mouse CD103	Biolegend	Cat#121420; RRID: AB_10714791
anti-mouse CD69	Thermo Fisher Scientific	Cat# 12-0691-82; RRID: AB_465732
anti-mouse Sca-1	Thermo Fisher Scientific	Cat# 17-5981-82; RRID: AB_469487
anti–mouse TNFα	Thermo Fisher Scientific	Cat#11-7321-82; RRID: AB_465418
anti–mouse IFNγ	Thermo Fisher Scientific	Cat#17-7311-82; RRID: AB_469504
anti-mouse/human granzymeB	Thermo Fisher Scientific	Cat# GRB17; RRID: AB_2536540
anti-mouse tbet	Thermo Fisher Scientific	Cat#50-5825-82; RRID: AB_10596655
anti-mouse eomes	Thermo Fisher Scientific	Cat# 46-4875-82; RRID: AB_10597455
anti-mouse blimp-1	Thermo Fisher Scientific	Cat# 12-9850-82; RRID: AB_2572738)
Anti-mouse CD3ε (purified)	Thermo Fisher Scientific	Cat# 16-0031-82; RRID: AB_468847
Anti-mouse CD28 (purified)	Thermo Fisher Scientific	Cat# 16-0281-86; RRID: AB_468923
anti-human CD8a	Thermo Fisher Scientific	Cat# 48-0088-42; RRID: AB_1272062
anti-human CD4	Thermo Fisher Scientific	Cat# 11-0049-42; RRID: AB_1659694
anti-human CD69	Thermo Fisher Scientific	Cat# 25-0699-42; RRID: AB_1548714
anti-human CD28	Thermo Fisher Scientific	Cat# 47-0289-42; RRID: AB_2573954
anti-human CD45RA	Thermo Fisher Scientific	Cat# 62-0458-42; RRID: AB_2744778
anti-human CD45RO	Thermo Fisher Scientific	Cat# 67-0457-42; RRID: AB_2717147
anti-human CD62L	Biolegend	Cat# 304806; RRID: AB_314466
anti-human CD27	Biolegend	Cat# 302832; RRID: AB_2562674
anti-human TNFa	Biolegend	Cat# 502906; RRID: AB_31525
anti-human CD25	Biolegend	Cat# 302614; RRID: AB_314284
anti-human IFNγ	Thermo Fisher Scientific	Cat# 12-7319-82; RRID: AB_1272026
anti-human tbet	Thermo Fisher Scientific	Cat# 12-5825-82; RRID: AB_925761
anti-human eomes	Thermo Fisher Scientific	Cat# 61-4877-42; RRID: AB_2574616
Bacterial and virus strains		
gB expressing Listeria monocytogenes	Orr et al., 2007	N/A
Wild type Listeria monocytogenes	Smithey et al., 2008	N/A

(*Continued on next page*)

Continued

Reagent or resource	Source	Identifier
gB expressing Vaccinia	Rudd et al., 2011	N/A
Biological samples		
Cord blood mononuclear cells	University of Rochester Pediatric Processing Core	N/A
Adult peripheral blood mononuclear cells	University of Rochester Pediatric Processing Core	N/A
Chemicals, peptides, and recombinant proteins		
gB (SSIEFARL) peptide	21st Century Biochemicals	Custom Synthesis
Recombinant murine IL-18	Thermo Fisher Scientific	Cat# PCM0184
Recombinant murine IL-12p70	Thermo Fisher Scientific	Cat# 14-8182-62
Recombinant murine IL-12p70	Peprotech	Cat# 210-12-50ug
Recombinant human IL-2	Thermo Fisher Scientific	Cat# 14-8029-81
Collagenase, type I	Worthington Biochemicals	Cat# CLS-1
DNase I	Roche	Cat# 10104159001
Calcium Ionophore (A23187)	Sigma Aldrich	Cat# C7522
LPS (Lipopolysaccharide)	Sigma Aldrich	Cat# L5418
Recombinant murine GM-CSF	Sigma Aldrich	Cat# GF026
PHA-L (Phytohemagglutinin-L)	Thermo Fisher Scientific	Cat# 00-4977-03
Brefeldin A	Thermo Fisher Scientific	Cat# B7450
CFSE Proliferation Dye	Thermo Fisher Scientific	Cat# C34554
Fixable Viability Dye	Thermo Fisher Scientific	Cat# 65-0865-14
Monensin	Thermo Fisher Scientific	Cat# 00-4505-51
Critical commercial assays		
Exofect Exosome Transfection Kit	Systems Biosciences	Cat# EXFT20A-1
IC fix perm buffer set	Thermo Fisher Scientific	Cat# 88-8824-00
Foxp3 fix/perm buffer set	BD biosciences	Cat# 554714
Human PrimeFlow RNA Assay Kit	Thermo Fisher Scientific	Cat# 88-18005-210
Human T cell Activation and Expansion Kit	Miltenyi	Cat# 130-091-441
Trizol	Thermo Fisher Scientific	Cat# 15596018
Deposited data		
Raw and analyzed data	This paper	GEO: GSE159688
Genome Reference Consortium Mouse Build 38, GRCm38/mm10	Genome Reference Consortium	GenBank: GCA_000001635.2
Genome Reference Consortium Human Build 38, GRCh38/hg38	Genome Reference Consortium	GenBank: GCA_000001405.15
Original code	This paper	Zenodo: https://zenodo.org/record/5564982
Experimental models: Cell lines		
B16-Flt3 mouse melanoma	Fulton et al., 2015	N/A
Experimental models: Organisms/strains		
B6 (C57BL/6J) mice	Jackson Laboratories	RRID: IMSR_JAX:000664
Thy1.1 (B6.PL-Thy1^{a} /CyJ) mice	Jackson Laboratories	RRID: IMSR_JAX:000406
Ly5.2 (B6-Ly5.1/Cr) mice	Charles River/NCI	RRID: IMSR_CRL:564
TCRa−/− (Tcra^{tm1Mom}/J) mice	Jackson Laboratories	RRID: IMSR_JAX:002116
CD4-Cre (B6.Cg-Tg(Cd4-cre) 1Cwi/BfluJ) mice	Jackson Laboratories	RRID: IMSR_JAX:022071

(*Continued on next page*)

Continued

Reagent or resource	Source	Identifier
miR-29ab-1 fl/fl mice	Smith et al., 2012	N/A
gBT-I mice	Mueller et al., 2002	N/A
Oligonucleotides		
miR29 guide strand: 5′-UAGCACCAUCUGAAAU CGGUUA-3′	This paper (Sigma-Aldrich)	N/A
miR29 passenger strand: 3′-ACCGAUUUCAGA UGGUGUGAAU-5′	This paper (Sigma-Aldrich)	N/A
Negative control guide strand: 5′-UAAAAAUCGC GUGGAUUAAUG-3′	This paper (Sigma-Aldrich)	N/A
Negative control passenger strand: 3′-UUAA UUUACGCGGUUUUUAUU-5′	This paper (Sigma-Aldrich)	N/A
RT-qPCR primers for miR-29 target genes, see Table S3	This paper (IDT)	N/A
RT-qPCR primers for hsa-miR-29a-3p	QIAGEN	YP00204698
RT-qPCR primers for hsa-miR-29b-3p	QIAGEN	YP00204679
RT-qPCR primers for hsa/mmu U6 snRNA	QIAGEN	YP00203907
RT-qPCR primers for cel-miR-39-3p	QIAGEN	YP00203952
Recombinant DNA		
Software and algorithms		
FlowJo 10.5.3	Tree Star	https://www.flowjo.com/solutions/flowjo
Prism 10	GraphPad Software	https://www.graphpad.com/scientific-software/prism/
Excel	Microsoft	N/A
BD Diva	BD Biosciences	https://www.bdbiosciences.com/en-us/products/software/instrument-software/bd-facsdiva-software#Overview
cellranger v3.1.0	Cell Ranger - 10x Genomics	https://support.10xgenomics.com/single-cell-gene-expression/software/pipelines/latest/what-is-cell-ranger
Seurat v3.2.2	Stuart et al., 2019	https://satijalab.org/seurat/index.html
Harmony	Korsunsky et al., 2019	https://github.com/immunogenomics/harmony
TargetScan v7.2	Agarwal et al., 2015	http://www.targetscan.org/mmu_72/
ENCODE ATAC-seq pipeline v1.1.7	ENCODE-DCC	https://www.encodeproject.org/atac-seq/
featureCounts v2.0.0	Liao, Smyth, and Shi, 2014	http://bioinf.wehi.edu.au/featureCounts/
DESeq2 v1.26.0	Love, Huber, and Anders, 2014	https://bioconductor.org/packages/release/bioc/html/DESeq2.html
EdgeR v3.28.1	Robinson, McCarthy and Smyth, 2010; McCarthy, Chen and Smyth, 2012	https://bioconductor.org/packages/release/bioc/html/edgeR.html
Morpheus	Broad Institute	https://software.broadinstitute.org/morpheus/
HOMER	Heinz et al., 2010	http://homer.ucsd.edu/homer/
JASPAR	Fornes et al., 2020	https://jaspar.genereg.net/
Analysis of Motif Enrichment (AME)	McLeay and Bailey, 2010	https://meme-suite.org/meme/doc/ame.html
MEME Suite	Bailey et al., 2009	https://meme-suite.org/meme/index.html
BaGFoot v0.9.7.2	Baek, Goldstein, and Hager, 2017	https://sourceforge.net/projects/bagfootr/
bamCoverage v3.4.3 in deepTools	Ramírez et al., 2016	https://deeptools.readthedocs.io/en/develop/index.html
bigWigMerge, bedGraphToBigWig	UCSC toolkit	http://hgdownload.soe.ucsc.edu/admin/exe/

(*Continued on next page*)

Continued

Reagent or resource	Source	Identifier
hisat2 v2.2.0	Kim et al., 2019	http://daehwankimlab.github.io/hisat2/
trim_galore	Babraham Bioinformatics	https://www.bioinformatics.babraham.ac.uk/projects/trim_galore/
Vertebrate Homolog	Mouse Genome Informatics	http://www.informatics.jax.org/homology.shtml
Irreproducibility Discovery Rate (IDR) v2.0.3	Li et al., 2011	https://github.com/nboley/idr, https://github.com/kundajelab/idr
MACS2 v2.1.1.20160309	Zhang et al., 2008	https://github.com/taoliu/MACS
SCTransform	Hafemeister and Satija, 2019	https://github.com/ChristophH/sctransform

RESOURCE AVAILABILITY

Lead contact

Further information and requests for resources and reagents should be directed to and will be fulfilled by the lead contact, Andrew Grimson (agrimson@cornell.edu).

Materials availability

This study did not generate new unique mouse lines or reagents.

Data and code availability

- RNA-seq, ATAC-seq and single cell RNA-seq data have been deposited at GEO and are publicly available as of the date of publication. Accession numbers are listed in the key resources table. All data reported in this paper will be shared by the lead contact upon request.
- All original code has been deposited at Zenodo and is publicly available as of the date of publication. DOIs are listed in the key resources table.
- Any additional information required to reanalyze the data reported in this paper is available from the lead contact upon request.

EXPERIMENTAL MODEL AND SUBJECT DETAILS

Biological samples

Human T cells

Frozen de-identified whole male adult (18-55 years of age) peripheral blood mononuclear cell samples and frozen deidentified male cord blood (39-41 weeks gestation) mononuclear cell samples were obtained from the University of Rochester Pediatric Processing Biorepository Core at the University of Rochester in accordance with University of Rochester's Committee on the Use of Human Subjects for Research as all samples were deidentified, and the research involved interaction with the donors in the NICU or voluntary donation.

Mice

C57Bl6, B6-Ly5.2/Cr mice were purchased from the National Cancer Institute colony, and B6-Thy1.1/CyJ CD4-Cre mice, B6/CyJ TCRa−/− mice and Thy1.1 B6.PL-Thy1a /CyJ mice were purchased from the Jackson Laboratory. MiR-29ab-1 fl/fl mice were generously provided by Dr. Stefan Costinean of Ohio State University and crossed to the B6-CyJ CD4-Cre mice. All mouse strains were crossed with gBT-I TCR homozygous transgenic mice (transgenic for TCR$\alpha\beta$ specific for the HSV-1 glycoprotein $gB_{498-505}$ peptide SSIEFARL) provided by Dr. Janko Nikolich-Zugich (University of Arizona, Tucson, AZ). All mice were sex matched as males at 8-12 weeks of age for adult group and 5-7 days old for neonate group and maintained under pathogen-free conditions at Cornell University's College of Veterinary Medicine. The experiments in this study were performed in strict accordance with the recommendations in the Guide for the Care and Use of Laboratory Animals of the National Institutes of Health and protocols reviewed and approved by the Institutional Animal Care and Use Committee at Cornell University.

Cell culture

B16-Flt3 mouse melanoma tumor cell line was provided by Dr. Stephen Jameson (University of Minnesota, MN) (Fulton et al., 2015). Cells were cultured in RP-10 (RPMI supplemented with 10% FBS) and passaged twice before experimental use. Conditioned media from each passage was also saved at −20°C in 50 mL aliquots for future experimental use.

METHOD DETAILS

Tissue distribution and vascular staining

For acquiring samples in the memory phase after infection, 3 μg of CD8b FITC in 100 μl PBS was injected intravenously into the retro-orbital sinus and left in circulation for 3 minutes before the animal is euthanized. For vascular stained memory and peak of infection samples, blood samples were obtained by retro-orbital bleed using a glass pipette. Mice were then euthanized and spleen, lymph nodes (cervical, mesenteric and inguinal), and lung or liver were removed. Single cells suspensions of spleen, and lymph node were made by manual dissociation and filtration through a 40 μm filter. Liver tissue was dissociated automatically using C tubes on a gentleMacs Dissociator (Miltenyi), then filtered through a 70 μm filter and hepatocytes removed by 3 slow centrifugal spins to further enrich for lymphocytes. Lung tissue was homogenized and digested using C tubes on a gentleMacs Dissociator with 0.5 mg/mL collagenase and 0.02 mg/mL DNase I in RP-10 for 30 minutes at 37°C followed by filtration through a 70 μm filter and ACK Lysis Buffer incubation to remove RBCs and enrich for lymphocytes. Following preparation of single cell suspensions, cells were stained directly or positively enriched for CD8s using CD8a microbeads then processed for flow cytometry.

Flow cytometry

All antibodies were purchased from Thermo Fisher Scientific or Biolegend. When fixation was required, the IC fixation and permeabilization kit from Thermo Fisher Scientific was used according to manufacturer's instructions. For intracellular staining, the BD FoxP3 fix/ perm buffer set was used. Flow cytofluorimetric data were acquired on an Attune with 4 lasers and a custom BD Symphony instrument equipped with five lasers using the DiVa software. Analysis was performed using the FlowJo software.

Adoptive single transfer experiments

Splenocytes were collected from congenically marked male adult and male neonate C57Bl6/Thy1.1 gBT-I CD45.2 mice and incubated with CD8a microbeads. Cells were then passed over an LS magnetic column, according to the manufacturer's instructions and CD8+ T cells were isolated via positive magnetic selection (~90%–95% purity). $1x10^4$ CD4Cre ± miR-29fl/fl gBT-I (KO/WT) or neonate CD8-enriched splenocytes from male donor mice were adoptively transferred (i.v.) into 10-12-week-old adult male B6-Ly5.2 CD45.1 recipient mice the day before infection. At indicated days post-infection, the proportion and phenotype of the donor cells in the blood were determined by flow cytometry.

Infections

Unless stated otherwise, mice were infected with Recombinant vaccinia virus expressing the gB-peptide, designated VACV-gB that was generously provided by Dr. S.S. Tevethia (Pennsylvania State University, College of Medicine). Mice were infected with $2x10^5$ PFU of VACV-gB (i.p.). For specific experiments, *Listeria monocytogenes* colonies were selected for growth in liquid culture and bacteria were grown to log phase. Mice were intravenously infected with $5x10^3$ CFU of either wild-type *Listeria monocytogenes* (strain 10403, obtained from Dr. Nikolich-Zugich, designated WT-LM), or a recombinant strain of *Listeria monocytogenes* expressing the gB-peptide (obtained from Dr. Sing Sing Way, designated LM-gB).

Dendritic cell IL-12 immunization

Adult male 8-10-week-old C57/Bl6 mice were subcutaneously injected with $5x10^6$ B16-Flt3 L cells after 2 cell culture passages. After 10-14 days, when skin tumors were visible, tumor mice were given LPS i.v (2 μg/mouse) to mature dendritic cells. The next day spleens were harvested and manually homogenized and run through a 40 μm filter. The spleen homogenate was resuspended in complete RPMI media containing rGM-CSF (50 ng/mL) with B16-Flt3L conditioned media in a 2:1 ratio, respectively with 1 μM SSIEFARL (gB) peptide for 5 hours at 37°C with constant gentle agitation. After the incubation period, dendritic cells were purified with CD11c microbeads using positive magnetic selection (~95% purity), according to the manufacturer's instructions. The isolated CD11c+ dendritic cells were counted, washed and $1x10^6$ gB loaded dendritic cells were injected i.v. into recipient B6-Ly5.2 mice for stimulation of Cre+/− miR-29 fl/fl gBT-I donor CD8+ T cells (KO/WT), which were adoptively transferred into CD45.1 recipient mice 24 hours prior. 24 hours after DC immunization, mice were injected with IL-12 i.p. (200 ng, 20 ng, 2 ng) or PBS for 4 days consecutively. Donor cells were assessed on day 5 after IL-12 priming.

PrimeFlow RNA Assay

Adult/neonatal mouse and human adult/cord male CD8+ T cells were enriched from mouse spleen homogenate and adult peripheral/cord blood mononuclear cells, respectively, via CD8a microbead positive magnetic selection. Purified CD8+ T cells were labeled with surface antibodies then fixed and permeabilized according to manufacturer's specifications as initial sample preparation. Cells were then incubated with customized Type 1 A647 miR-29a probe set or customized Type 1 internal positive control RPL13A probe set to achieve target hybridization. Signal amplification was achieved by further hybridization of preamplifier and amplifier DNA to target probe then fluorescently labeled probes were added for detection via flow cytometry. All steps followed by manufacturer's specifications in a 96-well plate.

Pathogen burden

20,000 CD8+ T cells enriched from spleen of Cre+ and Cre- miR-29 fl/fl gB+ (KO and WT respectively) male mice were singly transferred to male adult TCRaKO mice by i.v. injection. TCRaKO recipient mice were infected with $5x10^4$ cfu LM-gB i.v. within 24 hours then reinfected with $5x10^4$ cfu LM-gB i.v. 4 weeks later. 3 days after primary and secondary infection, spleen and liver were harvested, weighed and homogenized using the gentleMACS Dissociator in lysis solution (sterile deionized water with 0.02% NP-40 substitute). Spleen and liver homogenates were then serially diluted in sterile deionized water from 10-2 to 10-8 and 10 μl plated on strep BHI plates in quadruplet. BHI plates were then allowed to dry and incubated at room temperature for 3 days. Colonies were then enumerated using a counter manually by 2 lab personnel once visible and bacterial titer was calculated.

In vitro mouse proliferation assay

Spleens were harvested from male Cre+ and Cre- miR-29 fl/fl gBT-I mice (KO and WT) and filtered through a 40 μm filter to prepare single-cell suspensions. CD8+ T cells were purified using CD8α microbeads according to the manufacturer's protocol. The isolated CD8+ T cells were resuspended in PBS and labeled with CFSE at a 1:500 dilution. Cells were resuspended in media containing exogenous hIL-2 (2 ng/mL) and stimulated with either cognate peptide (SSIEFARL) (10^{-6} M and 10^{-9} M) in a 96-well round-bottom plate or plate-bound mouse anti-CD3ε (0.1 or 10 μg/mL) + soluble anti-CD28 (0.5 or 10 μg/mL) in a 96-well flat-bottom plate or plate-bound mouse anti-CD3ε (2 μg/mL) + soluble anti-CD28 (5 μg/mL) with IL-12 (0.2 or 20 ng/mL).

In vitro mouse gB peptide restimulation

Bulk splenocytes from infected mice at peak of infection were restimulated *in vitro* with 10^{-7} M gB peptide for 4 hours at 37°C in the presence of 3 μg/mL of Brefeldin A. Cells were then fixed and stained with both surface and intracellular antibodies for flow cytometric analysis of cytokine secretion.

In vitro mouse bystander activation

CD8+ T cells from Cre+ (KO) and Cre- (WT) miR-29 fl/fl gBT-I mice were isolated by positive magnetic selection using anti-CD8a microbeads according to manufacturer's instructions. Following isolation, cells were incubated in RP-10 with IL-2 alone (2 ng/mL) or IL-2 (2 ng/mL), IL-12 (20 ng/mL) and IL-18 (20 ng/mL) for 18 hours. After 18 hours, 3 μg/mL Brefeldin A was added to the cells and incubated for an additional 4 hours. Cells were then harvested, fixed and stained with both surface and intracellular antibodies for flow cytometry analysis of cytokine secretion.

PCR analysis of floxed miR-29ab1 locus

Genomic DNA was extracted from Cre+ (KO) and Cre- (WT) TN and VM nuclei using the QIAamp Fast DNA Tissue Kit (QIAGEN), following the manufacturer's protocol. 50 ng of genomic DNA was diluted 1:5 twice. PCR was performed using ExTaq polymerase (Takara Bio), following the manufacturer's protocol, with the forward primer 5′-TGTAAGCCTCGTGCTCACTG-3′ and the reverse primer 5′-ACCGTCAAATCTGCAACCCA-3′. Approximate percent excision was calculated using densitometry analysis of band intensity with Image Lab v6.0.1 (Bio-Rad Laboratories).

Quantitative RT-PCR (qRT-PCR)

Total RNA was extracted from naive CD8+ T cells using TRIzol following the manufacturer's instructions. For qRT-PCR of miR-29a and miR-29b, RT was performed using the miRCURY LNA RT Kit (QIAGEN), with 50-100 ng of total RNA as input and 1 attomole of cel-miR-39-3p from the miRCURY LNA Spike-In Kit (QIAGEN) spiked in, per the manufacturer's protocol. cDNA was diluted 1:50 in the qPCR reaction using the miRCURY LNA SYBR® Green PCR Kit (QIAGEN) following the manufacturer's protocol, denatured at 95°C for 2 min followed by 45 cycles of 95°C for 10 s and 56°C for 1 min on a LightCycler 480 (Roche). Forward and reverse primers for hsa-miR-29a-3p (YP00204698), hsa-miR-29b-3p (YP00204679), hsa/mmu U6 snRNA (YP00203907) and cel-miR-39-3p (YP00203952) were designed by QIAGEN. Data were normalized to the spike-in cel-miR-39-3p and housekeeping gene U6 snRNA, and analyzed by the 2-ΔΔCT method. For reverse transcription of miR-29 target mRNA genes, 150-250 ng of total RNA was incubated with 5 μg of dN9s (IDT) in a 12.5 μL reaction volume at 80°C for 5 min, followed by 60°C for 5 min. Then, 4 μL of RevertAid 5x Reaction Buffer (Thermo Scientific), 0.5 μL of RiboLock (Thermo Scientific), 2 μL of 10 mM dNTPs and 1 μL of RevertAid Reverse Transcriptase (Thermo Scientific) were added, and the reaction was incubated at 42°C for 1 hour, 70°C for 10 minutes and held at 4°C. For qPCR, the cDNA was diluted 1:50 and performed using SYBR Green master mix (Life Technologies) on a LightCycler 480 (Roche) by denaturing at 95°C for 2 min followed by 40 cycles of 95°C for 15 s, 59°C for 25 s and 72°C for 30 s. For qPCR primers, see Table S3. Data were normalized to the housekeeping gene PPIA and analyzed by the 2-ΔΔCT method.

RNA oligonucleotide sequences and modifications

The ssRNA miR-29a ASOs (5′-AUCGUGGUAGACUUUAGCCAAU-3′) and negative control ASOs (5′-AUUUUUAGCGCAC CUAAUUAC-3′) were synthesized with 2′-O-methyl modifications at every ribonucleotide by Sigma-Aldrich (USA). The dsRNA miR-29 mimics (guide strand: 5′-UAGCACCAUCUGAAAUCGGUUA-3′) (passenger strand: 3′-ACCGAUUUCAGAUGGUGUGA AU-5′) and negative control mimics (guide strand: 5′-UAAAAAUCGCGUGGAUUAAUG-3′) (passenger strand: 3′-UUAAUUUACGCG

GUUUUUAUU-5′) were synthesized by Sigma-Aldrich (USA) and annealed together by heating to 95°C for 5 min and slowly cooling to room temperature in 1x siRNA buffer (Dharmacon).

Human RBC EV generation, purification and characterization

One pint of Group O- blood was obtained from New York Blood Center from a healthy male donor less than 30 years old with no communicable diseases and CMV negative in New York region with informed consent and consent to the standard disease panel testing. All experiments with human blood samples were performed according to the guidelines and the approval of Cornell University Human Subjects Ethics committee. Whole blood was depleted of white blood cells using a leukoreduction filter (Haemonetics, USA) then allowed to rest for 2 weeks at 4°C with gentle agitation every 48 hours. RBCs were then separated from plasma by centrifugation. Isolated RBCs were diluted in RBC storage buffer (sterile filtered PBS with citric acid, sodium citrate, glucose, adenine, sodium chloride, mannitol and sodium hydrogen phosphate) and treated with 10 μM calcium ionophore overnight. To purify EVs, RBCs and cell debris were removed by three rounds of centrifugation at 600*g*-3,260*g* at 4°C. The remaining supernatant were vacuum filtered through a 0.45 μm pore membrane filter (Millipore). EVs were concentrated by using ultracentrifugation with a SW32Ti rotor (Beckman Coulter, USA) at 100,000*g* for 70 min at 4°C. EVs were resuspended in cold PB then layered above 5 mL 60% sucrose cushion (frozen at −80°C) and centrifuged at 100,000*g* for 16 h at 4°C using a SW32Ti rotor (Beckman Coulter) with reduced braking speed. The red layer of EVs was collected and washed once with cold PBS using ultracentrifugation in a SW32Ti rotor (Beckman Coulter) at 100,000*g* for 70 min at 4°C. All ultracentrifugation experiments were performed with a Beckman XE-90 ultracentrifuge (Beckman Coulter). Purified RBCEVs were resuspended in 3 mL PBS, aliquoted and stored at −80°C. The concentration and size distribution of EVs were quantified via dilution using a NanoSight Tracking Analysis NS300 system (Malvern, UK) provided by the Cornell Nanoscale Science and Technology Facility.

RBC-EV chemical transfection

Transfection of RBCEVs were performed using the Exofect Exosome Transfection kit (System BioSciences, USA). PBS, 10 μM oligo material (miR-29 ASO/NC ASO/miR-29 mimic/NC mimic), 2.5 μL Exofect solution and 25 μg RBCEVs were mixed to a final volume of 200 μL per well and incubated at 37°C with gentle shaking for 15 minutes. The RBCEV transfection solution was immediately transferred onto ice for 30 minutes. PBS was then added and samples were centrifuged for 30 min at 14,000*g* at 4°C in a table top fixed rotor centrifuge (Eppendorf) twice. Final pellet was resuspended in 100 μL of EV-free complete RPMI-1640 media with 10% FBS, Pen/Strep and L-glutamine per well.

In vitro EV nucleic acid treatment of naive mouse and human T cells

200,000 human or mouse magnetically enriched CD8+ T cells were plated in RPMI-1640 complete media with 10% FBS, Pen/Strep and L-glut with IL-7 (2 ng/mL) at a concentration of $2x10^6$ cells/mL as described below. 100 μL of RBCEV transfected media was added to each well and mixed well to break up any cell-EV aggregates. Cell and EV mixture was incubated at 37°C for 4-5 days and media was changed every 48 hours.

In vitro human TCR stim, proliferation and cytokine secretion assay

Frozen de-identified whole male adult (18-55 years of age) peripheral blood mononuclear cell samples and frozen deidentified male cord blood (39-41 weeks gestation) mononuclear cell samples were obtained from the University of Rochester Pediatric Processing Biorepository Core at the University of Rochester in accordance with University of Rochester's Committee on the Use of Human Subjects for Research as all samples were deidentified, and the research involved interaction with the donors in the NICU or voluntary donation. The frozen cord blood derived mononuclear cells and adult peripheral blood mononuclear cells were quick thawed, washed and rested in RPMI-1640 complete media for 12-16 hours. Human CD8+ T cells were isolated using positive magnetic selection by incubating with human CD8a microbeads. Cells were then passed over an LS magnetic column, according to the manufacturer's instructions and incubated with oligo loaded EVs as previously described above. After 5-day oligo-EV incubation, the isolated human CD8+ T cells were FACS sorted to acquire a 95% pure naive CD8+ cell population (CD45RA+, CD45RO–, CD27+, Viability lo). Sorted naive CD8+ T cells were resuspended in PBS and labeled with CFSE Proliferation Dye according to manufacturer specifications. Cells were then resuspended in media containing exogenous hIL-2 (2 ng/mL) and incubated with human biotin CD2, CD3 and CD28 beads from the T cell Activation/Expansion Kit (Miltenyi) according to manufacturer's instruction for 3 days. Complete media with IL-2 was changed every 48 hours. On Day 4, CD8+ T cells were resuspended in RPMI-1640 complete media containing 2 μg/mL PHA-L for 2 hours then incubated with 1x monensin and 3 μg/mL brefeldin-A for 4 additional hours. Three replicates of adult and three replicates of cord samples were used in the *in vitro* experiment. Cells were then harvested, fixed and stained with both surface and intracellular antibodies for flow cytometry analysis.

Mouse single cell RNA sequencing

Adult or neonatal mouse spleens were isolated in complete media and CD8+ T cells were positively selected for using magnetic microbead (Miltenyi) selection according to manufacturer's instructions. Splenic cells were then prepped for bulk naive CD8 FACS sorting on the SONY by staining with CD8, CD4 and Viability Dye (~97% purity) and 60,000 CD8+ cells sorted into PBS + 0.04% BSA. Sorted cells were then counted on a TC20 to capture 8,000 viable CD8+ T cells. Single cell 3′ RNA sequencing libraries were prepared by the Genomics core at Cornell University using a 10x Genomics Chromium instrument and the Chromium Single Cell 3′ Reagent kit

(v3), following the manufacturer's protocol. The libraries were sequenced on a NextSeq500 (Illumina) with 28bp+8bp index read and ~58 bp insert read lengths.

Human CD8+ sorting for RNA-seq

Adult or cord PBMCs were isolated in complete media and CD8+ T cells were positively selected for using magnetic microbead (Miltenyi) selection according to manufacturer's instructions. Cells were then prepped for naive CD8 subset FACS sorting on the SONY by staining with CD8, CD4, CD27, CD45RA and CD45RO and Viability Dye (~97% purity) and 100,000 CD8+ cells sorted into PBS + 2% BSA + 2 mM EDTA.

Mouse CD8+ sorting for RNA-seq and ATAC-seq

Adult or neonatal spleens were isolated in complete media and CD8+ T cells were positively selected for using magnetic microbead (Miltenyi) selection according to manufacturer's instructions. Cells were then prepped for naive CD8 subset FACS sorting on the SONY by staining with CD8, CD4, CD44 and CD122 and Viability Dye (~97% purity) and 200,000+ CD8+ cells sorted into PBS + 2% BSA + 2 mM EDTA.

Human/mouse RNA preparation and RNA sequencing

20,000 FACS sorted cells were placed in Trizol and RNA was extracted according to manufacturer's instructions, with the addition of a chloroform extraction, Glycoblue (ThermoFisher) carrier prior to precipitation (1 hour at 4°C), and a second wash of the pelleted RNA in 70% ethanol. RNA integrity was confirmed on a Fragment Analyzer (AATI). Libraries were prepared by the TREx core at Cornell University as follows: RNA-seq libraries were generated with the non-directional NEBNext Ultra II RNA Library Prep Kit (New England Biolabs) using total RNA isolated from 20,000 cells at 10 ng/μL. All RNA-seq libraries were sequenced with 85 nt single-end reads on a NextSeq500 (Illumina).

Mouse ATAC-seq nuclei prep, library preparation and sequencing

FACS sorted cells were permeabilized in lysis buffer (10 mM Tris-Cl pH 8.0, 300 mM sucrose, 10 mM NaCl, 2 mM $MgAc_2$, 6 mM $CaCl_2$, 0.2% NP-40 (Igepal), 0.5 mM DTT, 1x Pierce protease inhibitor (Thermo Scientific), and 40 units of RiboLock RNase inhibitor (Thermo Scientific) per 10 mL buffer) by brief aggressive pipetting, washed with buffer W (10 mM Tris-Cl pH 8.0, 300 mM sucrose, 10 mM NaCl, 2 mM $MgAc_2$, 0.008% Tween20, 0.5 mM DTT, 1x protease inhibitor, and 40 units of RiboLock RNase inhibitor per 10 mL buffer), and resuspended in storage buffer (50 mM Tris-Cl pH 8.3, 40% glycerol, 5 mM $MgCl_2$, 0.1 mM EDTA, 0.5 mM DTT, 1x protease inhibitor, and 40 units of RiboLock RNase inhibitor per 10 mL buffer). The cells were pelleted at 1000*g* for 8 minutes for each step of buffer change. The permeabilized cells were counted, snap-frozen in liquid nitrogen, and stored at −80°C. Libraries were prepared by the TREx core at Cornell University from 25,000 permeabilized cells as described in Buenrostro et al. (2015) and Corces et al. (2017). Briefly, frozen permeabilized cells were thawed, washed twice in ATAC-RSB buffer containing 0.1% Tween20, resuspended in Transposition Mix (Nextera DNA Sample Preparation Kit, Illumina) containing 0.1% Tween20 and PBS, and incubated for 30 minutes at 37°C with shaking (1000 rpm). After column cleanup, libraries were amplified using Nextera PCR oligos (Nextera Index Kit, Illumina) and Ultra II Q5 Master Mix (NEB) for a total of 12-14 PCR cycles based on qPCR quantification after the initial 5 cycles. The libraries were cleaned up twice (in series) with a 2:1 ratio of SPRIselect beads (Beckman Coulter). ATAC-seq libraries were sequenced with 75 nt single-end reads on a NextSeq500 (Illumina).

Single Cell RNA-seq analysis

Preprocessing

Fastqs were aligned to the mouse transcriptome (mm10) for each sample type using cellranger count in Cell Ranger pipelines (10x Genomics, v3.1.0). Cellranger aggr was then used to aggregate the multiple sample types with default parameters.

Data analysis

Data normalization, cell clustering, and differential expression were carried out using the Seurat R package v3.2.2 (Stuart et al., 2019). Cells with fewer than 200 genes or more than 15% of mitochondria genes were excluded from the analysis. Genes detected in fewer than 3 cells were also excluded from the analysis.

Integration was performed with Harmony R package (Korsunsky et al., 2019) and SCTransform (Hafemeister and Satija, 2019) in Seurat, respectively.

In Harmony integration, read counts were normalized using the Seurat NormalizeData function. Variable features used to downstream analysis were identified using the Seurat FindVariableFeatures function (nfeatures = 2000). Data was then scaled and centered using ScaleData function in Seurat. PCA was performed using the Seurat RunPCA function. Harmony integration was performed using RunHarmony function in Harmony R package. Uniform Manifold Approximation and Projection (UMAP) and Graph-based clustering (using the Seurat FindNeighbors and FindClusters functions) were performed with the top 20 principal components at the resolution of 0.5.

SCTransform was performed on cells of each sample type separately. SelectIntegrationFeatures was used to select features to use for integration (nfeatures = 3000). PrepSCTIntegration, FindIntegrationAnchors and IntegrateData were performed to integrate the data. Read counts were normalized using the Seurat NormalizeData function. PCA was performed using the Seurat RunPCA func-

tion. Graph-based clustering (using the Seurat FindNeighbors and FindClusters function) and UMAP was performed at the resolution of 0.3 with the top 20 principal components.

miRNA targeting signature

miRNA targets were defined as expressed genes (mean normalized read counts across cells > 0.01) with at least one target site for the particular miRNA with context++ score ≤ -0.2 in TargetScan (version 7.2) (Agarwal et al., 2015). The background set consisted of genes with at least one target sites of other conserved miRNAs, excluding all potential targets to the miRNA being tested. For cells in each identified cluster, log2 fold changes between WT and KO samples were calculated for miRNA targets and background genes separately. Distribution of log fold changes of the two groups of genes are compared using Wilcoxon test.

Marker genes

Marker genes for each cluster were identified using FindAllMarkers function in Seurat. Marker genes are genes that are identified to be expressed higher in the tested cluster than all other clusters. Normalized data matrix in RNA assay was used in differential expression testing. Genes detected in at least 10% of cells in the tested cluster or all other clusters are included, without requirements for fold differences between samples (logfc.threshold = 0). Only positive markers are returned. Default parameters were used unless described otherwise.

Differential expression

Differentially expressed genes are identified using FindMarkers function in Seurat. Genes detected in at least 10% of cells in either of the two populations are included, without requirements for fold differences between samples (logfc.threshold = 0).

For differential expression between samples, genes with adjusted p values smaller than 0.05 are classified as the differentially expressed genes. For differential expression within each cluster, genes with logFC greater than 0.05 are classified as the differentially expressed genes.

Gene set analysis

ImmGen clusters from Best et al. (2013) were used as gene sets for the gene set analysis. The pool of genes was the intersect of marker genes in all groups (when analyzing marker genes for each cluster), all genes included for differential expression (when analyzing differentially expressed genes between sample types) and genes in ImmGen gene sets. Two-sided Fisher exact test was used to test that whether the groups of genes were enriched with the ImmGen gene sets. P values from gene set enrichment tests on each group of genes were FDR-corrected.

ATAC-seq analysis

ATAC-seq read processing and peak calling

Raw sequencing reads were processed using ENCODE ATAC-seq pipeline (v1.1.7). Trimmed adaptor sequences were 'R1: CTGTCTCTTATACACATCT; R2: CTGTCTCTTATACACATCT'. Reads were mapped to the mouse genome (mm10). Paired-end mode was enabled and peak calling was performed using MACS2 v2.1.1.20160309 with '-f BEDPE' (https://github.com/taoliu/MACS) (Zhang et al., 2008). Irreproducibility Discovery Rate (IDR) v2.0.3 (Li et al., 2011) (https://github.com/nboley/idr, https://github.com/kundajelab/idr) analysis was enabled for cross-validation to compare replicates. Default parameters were used unless described otherwise. Reads were counted on each peak for all samples with featureCounts v2.0.0 (-p -F SAF -s 0 -Q 38) (Liao, Smyth and Shi, 2014).

Principle Component Analysis (PCA)

Peaks with mean Counts Per Million (CPM) across samples > = 1 are kept. Counts are transformed to log2 scale with rlog function in DESeq2 v1.26.0 (Love, Huber and Anders, 2014). PCA is performed using prcomp function in R.

Differential Accessibility

Read counts were normalized to CPM. Peaks with CPM > 1 in at least one sample were kept. Peaks with significantly more reads in one condition compared to another (FDR < 0.05) was identified using EdgeR v3.28.1(McCarthy, Chen and Smyth, 2012; Robinson, McCarthy and Smyth, 2010).

Clustering

Read counts are normalized to CPM and peaks with mean CPM across samples > = 1 are kept. Means of read counts for each sample type were taken across replicates. Counts were converted to z-scores across sample types (rowwise z-scores) prior to clustering analysis. Morpheus (Broad Institute) was used for k-means (k = 6) clustering and visualization by heatmaps.

Peak annotation

AnnotatePeaks.pl in HOMER (Heinz et al., 2010) was used to assign each peak to a nearest gene based on the shortest distance between the peak and gene's RefSeq transcription start site (TSS) in the mouse genome (mm10).

Gene set analysis

ImmGen clusters from (Best et al., 2013) were used as gene sets for the gene set analysis. The pool of genes was the intersect of genes associated with peaks included when identifying differentially accessible peaks (for analyzing genes associated with differentially accessible peaks), or genes associated with peaks in all six clusters (for analyzing genes associated with each cluster) and genes in all ImmGen gene sets. Two-sided Fisher exact test was used to test that whether the groups of genes were enriched with the ImmGen gene sets. P values from gene set enrichment tests on each group of genes were FDR-corrected.

Transcription factor motifs

Transcription factor binding profiles are obtained for from JASPAR (Fornes et al., 2020) CORE database v2020 (Vertebrates), with 746 non-redundant TF motifs.

Motif enrichment for transcription factor binding sites

Analysis of Motif Enrichment (AME) (McLeay and Bailey, 2010) in MEME Suite was used to identify motifs enriched in sequences of peaks more accessible in one condition relative to control sequences. Default parameters were used unless described otherwise. Control sequences were obtained from randomly subsetted insignificant peaks using fasta-subsample in MEME Suite (Bailey et al., 2009), and the number of subsetted control peaks was the mean of the numbers of significant peaks in both directions.

Transcription factor footprint identification

BaGFoot (Baek et al., 2017) was used to identify transcription factor activity. Prior to BaGFoot analysis, bam files of replicates were merged for each sample type.

Visualization

Bam files were normalized to RPKM using bamCoverage (v3.4.3, -bs 1) in deepTools (Ramírez et al., 2016). BigWig files for replicates of every sample type are merged using bigWigMerge (v2) and then sorted and converted to back bigwig format using bedGraphToBigWig in UCSC toolkit. Bigwig files are visualized using UCSC genome browser.

RNA-seq analysis

RNA-seq reads processing

Adaptors were trimmed from raw reads with trim_galore with default parameters (Babraham Bioinformatics: https://www.bioinformatics.babraham.ac.uk/projects/trim_galore/). Reads were mapped to the hg38 or mm10 genome with hisat2 v2.2.0 (Kim et al., 2019). FeatureCounts v2.0.0 (Liao, Smyth and Shi, 2014) was then used to counts mapped reads for genomic features using GENCODE human gene annotation v30 or mouse gene annotation v21 (-s 0 -Q 50). Peaks with mean Counts Per Million (CPM) across samples > = 1 are kept. Counts were transformed to log2 scale with *rlog* function in DESeq2 v1.26.0 (Love, Huber and Anders, 2014). PCA was performed using prcomp function in R.

Differential expression and gene set analysis

Raw counts were normalized to CPM values, and genes with CPM > 1 in at least one sample were kept for differential expression analysis. EdgeR v3.28.1(McCarthy, Chen and Smyth, 2012; Robinson, McCarthy and Smyth, 2010) was used to identify differentially expressed genes using likelihood ratio test.

Genes with p values smaller than 0.05 in differential expression analysis were classified as differentially expressed genes used in gene set analysis.

Human genes are first converted to their mouse homologs using Vertebrate Homolog data from Mouse Genome Informatics (MGI) (URL: http://www.informatics.jax.org/homology.shtml). ImmGen gene sets from (Best et al., 2013) were the gene sets used for the gene set analysis. The pool of genes was the intersect of all genes included for differential expression and genes in ImmGen gene sets. Two-sided Fisher exact test was used to test that whether the groups of genes were enriched with the ImmGen gene sets. P values from gene set enrichment tests on each group of genes were FDR-corrected.

QUANTIFICATION AND STATISTICAL ANALYSIS

Statistical analysis for flow cytometric data was performed using Prism 7 software (GraphPad). Error bars represent SD unless otherwise noted. The exact value of 'n' represents the sample size as biological replicates with respect to the number of mice or the number of human donors, as denoted in the figure legend. Significance was determined by unpaired t test, or one-way or two-way ANOVA, followed by multiple comparisons posttest, as indicated in the figure legends. Significance is denoted as follows: *$p \leq 0.5$ and **$p \leq 0.01$ ***$p \leq 0.001$ and ****$p \leq 0.0001$.